

Enhanced photocatalytic degradation of organic contaminants in water by highly tunable surface microlenses

Qiuyun Lu,[†] Lingling Yang,[‡] Pamela Chelme-Ayala,[‡] Yanan Li,[†] Xuehua
1 Zhang,^{*,†} and Mohamed Gamal El-Din^{*,‡}

[†]*Department of Chemical and Materials Engineering, University of Alberta, 9211 116
Street NW, Edmonton, Alberta, T6G 1H9, Canada*

[‡]*Department of Civil and Environmental Engineering, University of Alberta, 9211 116
Street NW, Edmonton, Alberta, T6G 1H9, Canada*

E-mail: xuehua.zhang@ualberta.ca; mgamalel-din@ualberta.ca

Abstract

Photocatalysis¹ is one of the dominant technologies used to enhance the efficiency of water decontamination with light-based treatments. However, the effectiveness of photocatalysts is usually limited by the irradiation conditions and the properties of the water matrix. In this work, we have demonstrated the capability of surface microlenses (MLs) as a clean technology for more efficient photocatalytic water decontamination. Random or ordered surface MLs were fabricated from simple polymerization of nanodroplets produced in a solvent exchange process. Both random microlenses (MLR) and microlenses array (MLA) could enhance the photocatalytic degradation efficiency (η) of four representative pollutants, including methyl orange (MO), norfloxacin (NFX), sulfadiazine (SFD), sulfamethoxazole (SMX), spiked in ultra-pure water, synthetic natural water, or real river water. By controlling the conditions of light treatment, η could be enhanced by up to 402 %. The effectiveness of surface MLs was validated under both visible LED light and simulated solar light and for two photocatalysts zinc oxide (ZnO) and titanium dioxide (TiO_2). By reducing the concentration of the photocatalysts from 100 to 5 mg/L and the intensity of irradiation intensity from 1 Sun to 0.3 Sun, our findings suggest that the enhancement factor by MLs was higher at lower catalyst concentration, or at lower light intensity. Based on optical simulations and experimental results, we demonstrated that surface MLs optimize the light distribution and promote the formation of active species, which results in the enhancement of η . The use of MLs may serve as a novel strategy to improve the photocatalytic degradation of micropollutants, especially in places where the available light source is weak, such as indoors or in cloudy regions.

Keywords: surface microlenses, microlens array, focus effect, photocatalysis, water decontamination

Synopsis: MLs-enhanced photocatalysis degradation of organic contaminants in different water matrices

27 Introduction

28 Photoreactions are widely applied in different fields,² such as data storage,^{3,4} display,⁵ light
29 generation,^{6,7} polymerization,^{8,9} and light-driven degradation.^{10,11} Many clean-energy tech-
30 nologies for water treatment benefits from photoreactions.¹² For instance, solar-based water
31 disinfection utilizes solar energy to inactivate or eliminate pathogenic contaminants in wa-
32 ter with portable containers, which is a low-cost and convenient method to provide safe
33 household water.^{13,14} In many types of photoreactions,¹⁵ photocatalysis, which is the pho-
34 toreactions accelerated by photocatalysts, is one of the dominant technologies to remove
35 the organic micropollutants in natural water.^{16,17} The most common type of photocatalysis
36 in water treatment is heterogeneous photocatalysis with semiconductor materials, such as
37 titanium dioxide (TiO_2)¹⁸ and zinc oxide (ZnO).¹⁹ The band gap of ZnO and TiO_2 can be
38 narrowed and be responsive to visible light.^{20,21} For example, the energy gap of ZnO reached
39 2.85 eV,²² while a TiO_2 -based catalyst had a band gap around 2.00 eV.²³ The action spec-
40 tra of ZnO and TiO_2 also confirmed their response under visible light and solar light.²⁴⁻²⁶
41 However, the application of photoreactions is often limited due to the inefficient utilization
42 of light.²⁷

43 One of the main reasons that restrict the development of solar-driven photocatalytic
44 degradation of organic pollutants in the aqueous environment is the instability of solar light
45 under different scenarios.^{28,29} For example, sunlight is attenuated when the wastewater has
46 high turbidity³⁰ or the rainy and cloudy weather appears.³¹ As a result, the number of
47 photons that can be absorbed into the system decrease, so the activity of photocatalysts is
48 considerably inhibited. In order to maximize the potential of photocatalysts under insuffi-
49 cient light, strategies to increase the number of species undergoing a photo process with a
50 given amount of photons are needed. Several strategies have been widely investigated for
51 this purpose, including incorporating light engineering design in photoreactors to improve
52 their performance,^{32,33} establishing a flow reactor to enhance the mass transfer or to shorten
53 the light path,³⁴ and preparing engineering photocatalytic materials for more efficient photo-

54 catalysis.³⁵ Introducing lenses into photoreaction systems is a potential alternative because
55 of the ability of lenses to redistribute light.³⁶ The focusing effect of a lens creates high local
56 light intensity at the focal point, accelerating the local photoreaction rates.

57 Surface microlenses (MLs) are novel lenses with small dimensions and a large number
58 fabricated on a solid surface.^{37,38} There are several advantages from surface MLs in a photore-
59 action process. First of all, surface MLs can be integrated into various reactors due to their
60 small dimensions.^{39,40} Besides, such lenses have short focal distances with strong near-field
61 focusing effect.^{41,42} Last but not the least, the MLs with well-controlled optical properties and
62 good durability can be prepared and flexibly modified by various methods.^{43,44} Commonly
63 used fabrication methods include laser writing,^{45,46} hot embossing,^{47,48} soft lithography,^{49,50}
64 and drop-templating.^{51,52} The fabrication of surface MLs based on nanodroplet polymeriza-
65 tion is one of the promising technologies that are highly tunable and affordable.⁵³ Through
66 this method, surface nano-/microlenses are obtained after the polymerization of surface
67 droplets formed in a solvent exchange.⁵⁴ Notably, the morphology and spatial arrangement
68 of surface nano-/microlenses are tunable⁵⁵ with the method, and the functional components,
69 such as plasmonic nanoparticles,⁴² can be introduced into the system conveniently.

70 In the work conducted by Dongare et al,⁵⁶ the feasibility of integrating lenses with light-
71 driven membrane devices for water purification was demonstrated, where a higher energy
72 conversion rate of the device was achieved because of the focus effect of lenses. On a smaller
73 scale, the acceleration of the photoreactions by surface MLs was validated through the in-situ
74 photoreduction of silver nitrate⁴² and the direct photolysis of micropollutants.⁵⁷ Therefore,
75 such surface MLs are also expected to be effective in enhancing the solar-driven photocat-
76 alytic degradation of contaminants in water. Implementing surface MLs based on the solvent
77 exchange process as a candidate strategy for enhancing photodegradation efficiency under
78 insufficient irradiation is worthy of investigation. However, the mechanisms of photocat-
79 alytic degradation combined with surface MLs have not been explored, so as the influence
80 of the properties of MLs, photocatalysts, light sources, and water matrix on the degradation

81 process.

82 In this work, we evaluated the performance of surface MLs in enhancing the photocat-
83 alytic degradation of four typical organic pollutants in river water, including methyl orange
84 (MO), norfloxacin (NFX), sulfadiazine (SFD), and sulfamethoxazole (SMX).⁵⁸⁻⁶⁰ Surface
85 MLs were photopolymerized from the nanodroplets obtained in a solvent exchange process⁶¹
86 and could be flexibly tailored for better performance. The optimized spatial arrangement
87 of surface MLs was selected based on the light treatment results. The mechanisms of sur-
88 face MLs-assisted photocatalytic degradation were investigated with experiments and optical
89 simulation. By tuning the light sources, irradiation intensity, water matrices, and the ge-
90 ometry of reactors, the practical conditions with limited irradiation were simulated where
91 the influence of surface MLs on photocatalytic degradation efficiency is studied. Last but
92 not the least, we used two commercial photocatalysts with good stability and durability,^{62,63}
93 ZnO and TiO_2 , to assess the applicability of surface MLs in varied catalytic processes. The
94 capability of surface MLs in promoting the photocatalytic degradation of organic pollutants
95 in water was validated.

96 **Experimental section**

97 **Fabrication and characterization of random surface microlenses and** 98 **high-curvature microlens array on planar glass substrate**

99 Surface microlenses (MLs) were fabricated by photopolymerization of surface droplets under
100 UV light, as shown in Figure 1 (a). The size and spatial distribution of surface MLs were
101 determined by the diameters and positions of surface droplets. The solvent exchange process
102 enabled us to flexibly control the formation of surface droplets and further adjust the proper-
103 ties of surface MLs.^{53,64} In the solvent exchange process, a self-assembled chamber was filled
104 with a solution (solution A) which was a mixture of monomer, photoinitiator, ethanol, and
105 Milli Q water. Then, Milli Q water saturated with monomer and initiator (solution B) was

106 inserted into the chamber at a fixed flow rate. Consequently, surface droplets composed of
107 monomers and the photoinitiator formed on the substrates due to the oversaturation during
108 the solvent exchange process. When the substrate was homogeneously hydrophobic, surface
109 droplets grew and coalesced on the substrate, leading to the formation of surface MLs with
110 non-uniform size and spatial distribution (random MLs, MLR) after UV curing. On the
111 other hand, surface droplet arrays (MLAs) could be prepared on a pre-patterned substrate
112 with ordered hydrophobic microdomains.⁵⁵

113 Random surface MLs (MLR) for photocatalytic degradation system were prepared us-
114 ing methyl methacrylate (MMA) ($\geq 98.5\%$, Alfa Aesar) as the monomer and 2-hydroxy-
115 2-methylpropiophenone (96%, Fisher) as the photoinitiator. Solution A was prepared by
116 adding 8.0 vol% MMA and 0.8 vol% photoinitiator in 40 vol% ethanol aqueous solution.
117 Then, Milli Q water saturated with MMA and photoinitiator, namely solution B, was in-
118 jected into the chamber at a flow rate of 50 mL/h. A glass slide homogeneously hydropho-
119 bized with octadecyltrichlorosilane (OTS) (98.9%, Acros Organics, Fisher Scientific) was
120 placed on top of the chamber as the substrate for surface droplets and MLs. The OTS
121 coating of the substrate was prepared according to the procedure described by Zhang and
122 Ducker.⁶¹ The condition used to fabricate the random surface MLs was the optimized one in
123 our previous work.⁵⁷ After the standard solvent exchange process, the chamber filled with
124 liquid was sealed and horizontally set under UV light (365 nm, Analytik Jena UV lamp) for
125 15 min.

126 Surface ML arrays (MLAs) in the photodegradation processes were fabricated with lauryl
127 methacrylate (LMA, Acros Organics) as the monomer in solution A. The solubility of LMA
128 in water was lower than MMA, leading to more stable surface droplets during the solvent
129 exchange and uniformity of surface MLAs. The pre-patterned substrate used for droplet
130 formation was decorated with circular hydrophobic microdomains arranged in an array, fab-
131 ricated by a photolithography process on an OTS-coated glass slide.⁵⁵ The diameter of each
132 circular domain was 5.0 μm , and the spacing between two adjacent domains was 2.5 μm .

133 By repeating the process of solvent exchange and UV curing, MLAs with higher curvature
134 could be achieved.⁶⁵ In this work, three rounds of solvent exchange-UV curing process were
135 performed. Solution A for the solvent exchange process was prepared by adding LMA and
136 the photoinitiator (1/10 volume of LMA) into ethanol, while solution B was the LMA and
137 photoinitiator saturated water. The LMA concentration in solution A in the three rounds of
138 solvent exchange was 2 vol%, 4 vol%, and 2 vol%, respectively, while the flow rate of adding
139 solution B into solution A was 8 mL/h, 4 mL/h, and 4 mL/h, correspondingly. The UV cur-
140 ing step lasted for 15 min after each round of the solvent exchange process, after which the
141 high-curvature poly(lauryl methacrylate) (PLMA) MLs were obtained. The curvature of the
142 PLMA ML array could not further increase because the adjacent MLs would be connected
143 if more LMA were added on top of the MLs base.

144 Surface random MLs and ML arrays were observed under an optical microscope equipped
145 with a camera (Nikon H600l and Nikon DSFi3). The lateral size and surface coverage rate of
146 MLs were calculated by analyzing optical photos with Image J. The height of random MLs
147 and high-curvature MLs array was separately characterized with atomic force microscope
148 (AFM, Bruker, tap mode) and confocal microscope (Zeiss Axio CSM 700). A transmission
149 mode confocal microscopy (Leica SP8) was applied to measure the focal distance of MLs
150 in the array. An intensity profile was obtained after a vertical scanning of the ML array-
151 decorated substrate. The focal distance was defined as the distance between the brightest
152 point in the intensity profile and the substrate surface.

153 **Fabrication and characterization of MLs-decorated glass vials**

154 The surface MLs can also be immobilized on a curved surface. The inner surface of a glass
155 vial (Fisherbrand Class A clear glass vial) with a volume of 30 mL was hydrophobized by
156 coating OTS onto the surface. The vial with a hydrophobic inner surface was firstly filled
157 with 12 mL of a solution (solution A) composed of 7.6 vol% MMA, 0.8 vol % photoinitiator,
158 45.8 vol% water, and 45.8 vol% ethanol. Then, Milli Q water saturated with MMA and

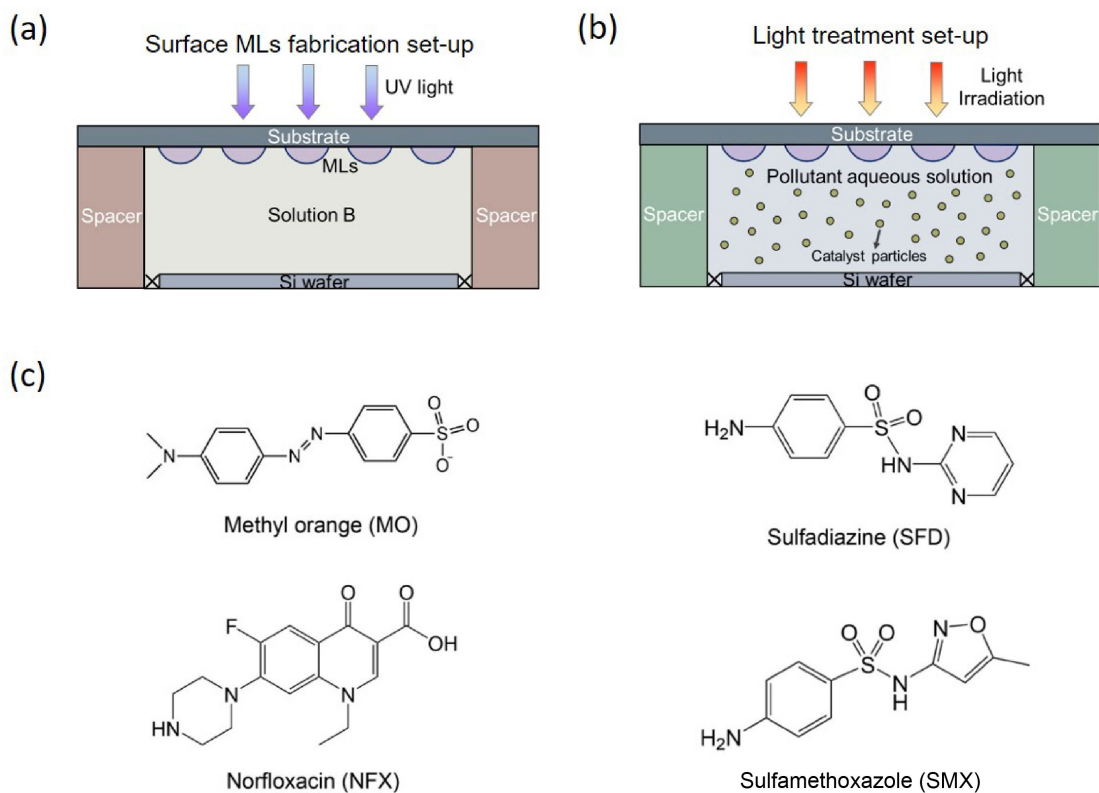


Figure 1: (a) Sketch of the fabrication process of surface MLs. The chamber height is 0.57 mm, the width is 12.2 mm, and the length is 56.0 mm (b) The experimental setup of light treatment with surface MLs and distributed catalysts particles. (c) Chemical structures of photodegraded pollutants, including methyl orange (MO), norfloxacin (NFX), sulfadiazine (SFD), and sulfamethoxazole (SMX)

159 photoinitiator (solution B) was dripped into the standing vial through two tubes and two
160 syringe pumps. The ends of the tubes were set at the opening of the vial, on the left side
161 and right side of the vial, respectively. The flow rate in each tube was fixed at 3 mL/min.
162 To fully replace solution A, 80 mL of solution B was added to the vial. During the solvent
163 exchange process, the excess liquid was discharged from the vial from the opening. After
164 the solvent exchange process, the vial was sealed and set under the UV lamp for 20 min.
165 After removing all remaining mixtures and the washing step, the PMMA MLs-decorated vial
166 was prepared. The morphology of the MLs-decorated vial can be observed with an optical
167 microscope. All the parameters mentioned above were optimized in our previous work.⁵⁷

168 **Optical simulations of surface MLs on planar substrates**

169 The optical simulations of surface MLs on planar substrates were conducted with Zemax
170 OpticStudio. The glass substrate decorated with MLs was set in a horizontal plane (X-Y
171 plane). A plane wave light source was set perpendicular to the horizontal plane (along the
172 Z axis) with an intensity of 21.64 W/cm^2 . Five horizontal light-flux detectors were set at
173 different depths in the solution below the MLs-decorated substrate to demonstrate the top-
174 view light irradiation profiles of both MLR and MLA. A rectangular X-Z plane monitor
175 which crossed through the center of a single ML in the array was also designed to describe
176 the cross-sectional irradiation profile of the ML.

177 **Photocatalytic degradation of pollutants with surface MLs**

178 The surface MLs were utilized in the photocatalytic degradation of common pollutants in
179 natural water and wastewater to enhance the photodegradation efficiency (η). To evaluate
180 the performance of random MLs and high-curvature ML array, the planar substrate with
181 immobilized surface MLs was assembled in a homemade chamber for the light treatment of
182 water that contained pollutants.(Figure 1 (b)) The light treatment was also conducted in
183 the PMMA MLs-decorated glass vials to evaluate the efficiency of MLs on a curved surface

184 on a larger scale. The pollutants involved in the degradation experiments include methyl
 185 orange (MO, 85%, Sigma-Aldrich), norfloxacin (NFX, Alta aesar), sulfadiazine (SFD, 99.0-
 186 101.0%, Sigma Aldrich), and sulfamethoxazole (SMX, analytical standard, Sigma Aldrich).
 187 The aqueous solutions of these pollutants with the analyte concentration of 5 mg/L were
 188 prepared with ultra-pure water (produced by Milli-Q Direct 16), synthetic river water, or
 189 real river water as the solvent. For the solution with ultra-pure water as the solvent, the pH
 190 value was measured at around 7 with a pH meter (Accumet AE150, Fisher Scientific).

191 To prepare the synthetic river water, 52.19 mg $Na_2SO_4 \cdot 10H_2O$ (Sigma Aldrich), 4.08 mg
 192 $NaNO_3$ ($\geq 99.0\%$, Sigma Aldrich), 106.96 mg $CaCl_2 \cdot 10H_2O$ (Sigma Aldrich), 100.81 mg
 193 $NaHCO_3$ (certified ACS, Fisher Chemical), 101.30 mg $MgSO_4 \cdot 7H_2O$ (Fisher BioReagents),
 194 2.56 mg humic acid (technical grade, Aldrich), and 5.32 mg alginic acid (Acros organics) were
 195 dissolved in 1 L ultra-pure water. The real river water was collected from Whitemud Creek
 196 to the North Saskatchewan River in Edmonton, Alberta, Canada at 9:30 am on April 26,
 197 2022. Both the synthetic water and real river water were characterized by a total organic
 198 carbon (TOC) analyzer (TOC-L Series, SHIMADZU), a pH meter (Accumet AE150, Fisher
 199 Scientific), and ion chromatography (Dionex ICS-5000, Thermo Scientific). The synthetic
 200 river water was at a pH value of 7.3, with a TOC value of 3.8 mg/L, and a COD value of
 201 9.2 mg/L, while the river water was at a pH of 7.5, a TOC value of 25.6 mg/L, and a COD
 202 value of 163.3 mg/L. The concentrations of ions in the synthetic are displayed in Table 1.
 203 SMX and MO were spiked in the synthetic river water and the real river water for the light
 204 treatment with the same concentration of 5 mg/L.

Table 1: Concentration of ions in the synthetic water (Unit: mM)

Ion type	SO_4^{2-}	Cl^-	NO_3^-	Na^+	Ca^{2+}	Mg^{2+}
Conc./mM	8.3	5.3	0.046	2.1	0.85	0.47

205 One of the commercialized photocatalysts, zinc oxide (ZnO, certified ACS powder, Fisher
 206 Chemical), was dispersed in the aqueous solutions containing different types of pollutants

207 by a sonication step for 20 min. All the solutions were stored in a dark environment at a
208 temperature of 4 °C except the light treatment process. The catalyst was dispersed in the
209 aqueous solutions with sonication in the dark environment for 30 min to ensure sufficient
210 adsorption of the pollutant on the surface of the catalysts. To assess the performance of
211 surface MLs with varied amounts of ZnO, multiple concentrations of ZnO dispersed in the
212 pollutant solutions (ultra-pure water as the solvent) were used, including 5 mg/L, 10 mg/L,
213 50 mg/L, and 100 mg/L. In addition to ZnO, titanium dioxide (TiO_2 , 21 nm primary particle
214 size, $\geq 99.5\%$, Aldrich chemistry) was used to verify the efficiency of surface MLs under
215 different types of catalysts. To compare the performance of MLs when using two types
216 of catalysts, the initial concentrations of TiO_2 and ZnO were set at 5 mg/L. The band
217 gap of ZnO and TiO_2 was 3.26 eV and 3.25 eV, respectively, which were measured with
218 diffusion reflectance spectrum (Hitachi U-3900H) and Tauc plot (shown in Supplementary
219 information, Figure S1 (c-d)).⁶⁶

220 Both the visible LED lamp (SOLIS-3C, Thorlabs) and the simulated solar light (SS200AAA
221 Solar Simulation Systems, Photo Emission Tech) were used as light sources for the photo-
222 catalytic degradation of pollutants in water. The distance between the upper surface of the
223 reactor and the light source was fixed at 23.5 cm for the visible light LED and 35.7 cm for
224 the simulated solar light. A series of irradiation conditions (shown in Table 2) were tested
225 in this work by changing the light sources, the glass substrate, and the type of surface MLs.
226 The spectra of the irradiation above the reactors were collected with a portable spectrometer
227 (StellarNet Inc) at the top position of reactors, as shown in Figure 2 (a). In order to assess
228 the influence of the irradiation conditions listed in Table 2 on the irradiation exposed to the
229 treated solution, the spectra of light that transmitted through the top surface of the reactor
230 (Figure 2 (b-g)) were obtained by setting the detection sensor of a spectrometer under the
231 top surface of different reactors. The light intensities of the light sources were adjusted to in-
232 vestigate the influence of the light intensity on the MLs-enhanced photocatalytic degradation
233 process.

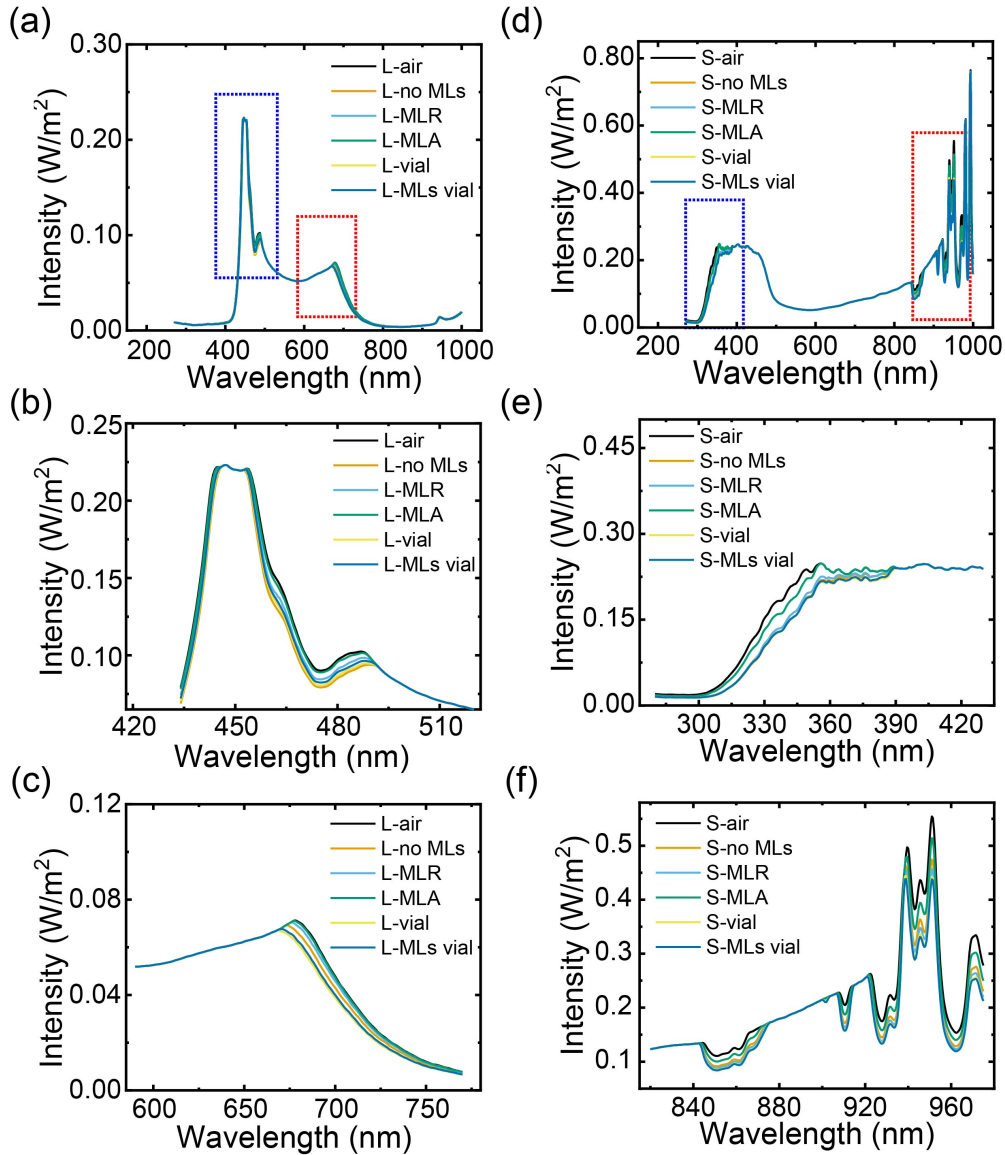


Figure 2: Spectra of light from visible LED lamp (intensity: 21.64 W/m^2) and from simulated solar light (intensity: 1 Sun) at the position of light treatment reactor. (a) Spectra of light from the visible LED lamp after transmitting through the air or top surface of the reactor. The zoomed-in spectra are shown in (b) (from 415 to 515 nm) and (c) (from 585 to 775 nm). (d) Spectra of the light from simulated solar light after transmitting through the air or the top surface of the reactor. The zoomed-in spectra are shown in (e) (from 285 to 435 nm) and (f) (from 820 to 775 nm).

Table 2: Irradiation conditions

Name C_0	Light source	Substrate type	MLs type
L-air		/	/
L-no MLs		Planar glass substrate	/
L-MLR	Visible LED	Planar glass substrate	MLR
L-MLA		Planar glass substrate	MLA
L-vial		Glass vial	/
L-MLs vial		Glass vial	MLR
S-air		/	/
S-no MLs		Planar glass substrate	/
S-MLR	Simulated solar	Planar glass substrate	MLR
S-MLA		Planar glass substrate	MLA
S-vial		Glass vial	/
S-MLs vial		Glass vial	MLR

234 All the light treatments involved in this study are summarized in Table 3, and each con-
235 dition is represented with its irradiation condition (listed in Table 2), the type of catalysts,
236 and the concentration of catalyst (unit: mg/L). The MLs-involved photocatalytic degrada-
237 tion process was studied by various analytical instruments. The degradation efficiency (η)
238 is calculated based on the equation (1), where C_i is the initial concentration of a pollutant
239 after the adsorption of pollutants reached equilibrium and C_f is the final concentration of
240 the pollutant after the light treatment. For the solution containing pollutants prepared
241 with ultra-pure water, the concentration change of a pollutant could be identified with UV-
242 visible spectroscopy (UV-vis, Thermo fisher, Genesys 150) based on the Beer-Lambert Law.
243 According to the Beer-Lambert Law, the absorbance (A) of an analyte in the solution is pro-
244 portional to its concentration (C) if the analyte concentration is within a linear range. The
245 relationship between absorbance and concentration is shown in (2) (ϵ : molar attenuation
246 coefficient, L: light path). The concentrations of organic analytes involved in this work are
247 within the linear range, and the evidence was included in the supporting information (Figure
248 S1). Therefore, the η of a pollutant can be calculated by equation (3) by combining equation
249 (1) and (2). A_i and A_f are the absorbance at the representative peak⁶⁷ of a pollutant before

Table 3: Conditions of light treatment

Light source	MLs type	Catalyst	Catalyst Conc. (mg/L)
Visible LED	MLR	/	/
	MLA	/	/
	/	ZnO	100/50/10/5
	MLR	ZnO	100/50/10/5
	MLA	ZnO	100/50/10/5
	/	TiO_2	5
	MLR	TiO_2	5
	MLA	TiO_2	5
Simulated solar	/	ZnO	100/10
	MLR	ZnO	100/10
	MLA	ZnO	100/10
	vial	ZnO	10
	MLs vial	ZnO	10

250 and after the treatment, respectively.

$$\eta = \frac{C_i - C_f}{C_i} \times 100\% \quad (1)$$

$$A = \varepsilon CL \quad (2)$$

$$\eta = \frac{C_i - C_f}{C_i} \times 100\% = \frac{A_i - A_f}{A_i} \times 100\% \quad (3)$$

251 For the solution containing pollutants prepared with the synthetic water, the concentra-
 252 tion changes of analytes were characterized by an ultra-performance liquid chromatography-
 253 mass spectrum (UPLC-MS, ACQUITY UPLC H-Class, Waters). The method to detect SMX
 254 with UPLC-MS was included in supporting information. All solutions containing photocat-
 255 alyst suspends were centrifuged for 10 min at 14,000 rpm, and then only the supernatant
 256 was used for analysis.

257 The performance of the photocatalysts is influenced by many factors associated with the

258 irradiation conditions (such as intensity, photon absorption, light scattering, etc.), catalyst
259 properties, adsorption of pollutants, properties of water matrices, and chemical properties
260 of organic contaminants. In order to show the enhancement of photocatalytic degradation
261 efficiency obtained by implementing surface MLs, all the parameters except the usage of MLs
262 were kept constant. The ability of surface MLs to enhance η of pollutants was quantified
263 with an enhancement factor (f) which was defined by the equation (4)

$$f = \frac{\eta_{(MLs+catalyst)}}{\eta_{catalyst}} \quad (4)$$

264 The reaction mechanisms may be further understood from the balance between the mass
265 of CO_2 generated from the complete degradation of organic contaminants and the mass
266 decrease in solutions containing contaminants.^{68,69} However, as shown in Figure 1 (b), our
267 reaction systems were fully sealed with negligible mass transfer from the system during the
268 irradiation. In addition, it was almost impossible to quantify the CO_2 production from our
269 systems due to the small volume of our samples and the dissolution of CO_2 in water. The total
270 amount of the model contaminant in the treated solution was 10 μg . Even from complete
271 degradation, only 17 to 22 μg CO_2 would be produced at maximum. CO_2 production from
272 the photodegradation of organic contaminants in MLs-enhanced photocatalytic systems may
273 be conducted in the future after modification of the experimental set-up. Instead of mass
274 balance to monitor the reaction mechanism, the characterization of free radicals generated in
275 the photocatalytic system was feasible to reveal the degradation mechanism in the presence
276 of surface MLs.^{70,71}

277 The presence of free radicals in the photocatalytic degradation process was verified with
278 an electron spin resonance (ESR) spectrum (Elexsys E-500, Bruker). The ultra-pure water
279 dispersed with ZnO (10 mg/L) was irradiated by the visible LED lamp or the simulated
280 solar light for 30 min before the ESR detection. 5,5-Dimethyl-1-pyrroline N-oxide (DMPO,
281 Sigma Aldrich), as a spin-trapping agent, was used to capture the hydroxyl free radicals
282 in the treated solution. DMPO was added to the treated solution with a concentration of

283 5.7 g/L just before the light treatment started. The solution was added into quartz (CFQ)
284 EPR tubes (outside diameter: 5mm) to detect free radical signals immediately after the
285 irradiation. The ESR spectrum of methanol dispersed with ZnO (10 mg/L) under MLA was
286 also obtained after the irradiation by simulated solar light for 30 min (shown in supporting
287 information, Figure S2).

288 **Results and discussion**

289 **Morphology and optical properties of MLs**

290 The redistribution of light irradiation is determined by the morphology and spatial arrange-
291 ment of surface MLs. The MLs on the pre-patterned substrate (MLA) are arranged in a
292 highly-ordered array with a uniform radius of $6.5 \mu\text{m}$ due to the confinement of hydrophobic
293 domains, as shown in Figure 3 (b). The surface coverage rate and the contact angle of MLA
294 are 49° and 63.7%, respectively. The light intensity profiles of MLA obtained from the
295 confocal microscope and optical simulation results of a single ML from the ML array are
296 displayed in Figure 3 (c) and (d), respectively. Due to the uniform size, the focal distances
297 of MLs in the array have the same value. From the light intensity profiles, it is found that
298 the focal points of MLA are located in a horizontal plane which is around $16 \mu\text{m}$ away from
299 the substrate. As a comparison, the focal distance of a single ML in the array is $16.5 \mu\text{m}$
300 according to the optical simulations. Therefore, the simulated focal distance is consistent
301 with that obtained from the confocal microscope.

302 Another type of surface MLs, represented with MLR, is fabricated on homogeneous sub-
303 strates. MLR are randomly distributed on the planar substrate, and their diameters vary
304 from $2 \mu\text{m}$ to $200 \mu\text{m}$ with a fixed contact angle of 7.5° . The surface coverage rate of MLR
305 is 47.2%. The focal distances of MLR differ due to the existence of the size distribution
306 among them. Therefore, it is difficult to measure the focal distances of MLR with a confocal
307 microscope.

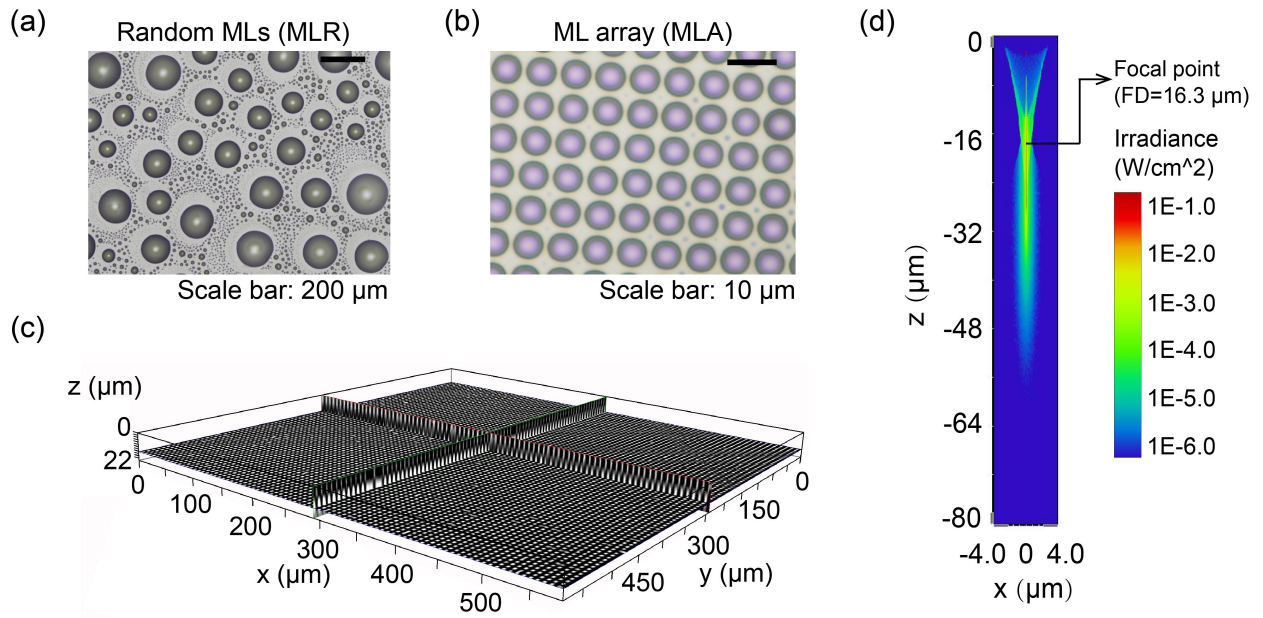
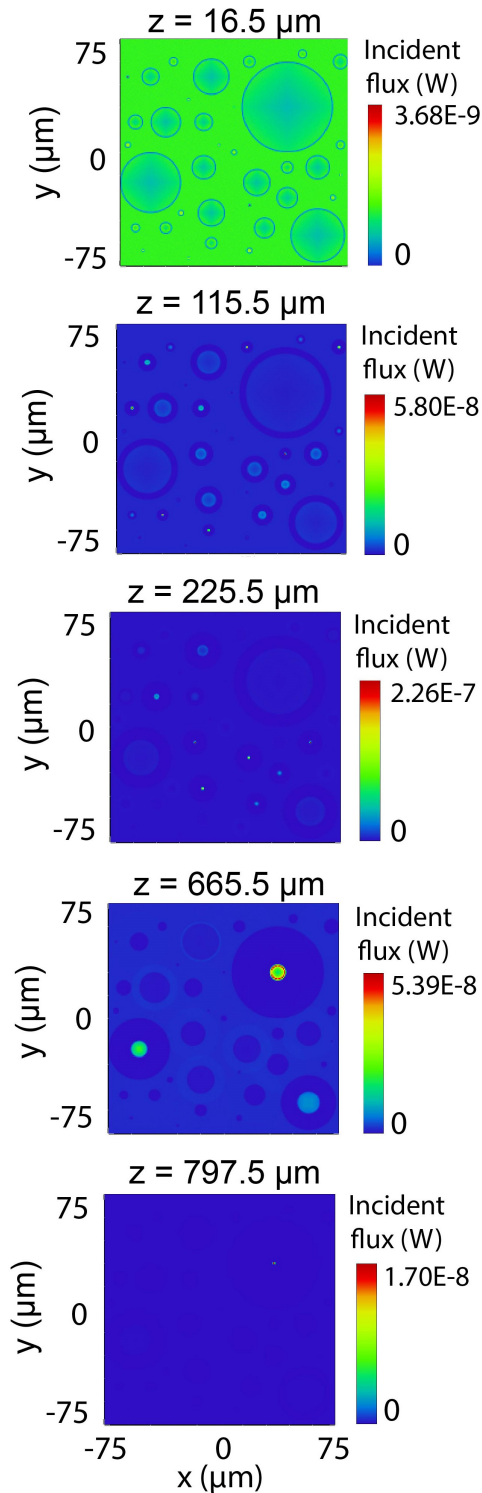


Figure 3: Images of (a) random MLs (scale bar: 200 μm) and (b) ML array (MLA) (scale bar: 10 μm) obtained with optical microscope (c) The light intensity profile of MLA with confocal microscope (scale bar: 100 μm) (d) The cross-sectional light intensity of a single ML in the array. The point with the highest irradiance value is the focal point. The position with $z=0$ is the substrate surface. The focal distance is the distance between the focal point and the substrate surface.

(a) MLR Top-view intensity profiles



(b) MLA Top-view intensity profiles

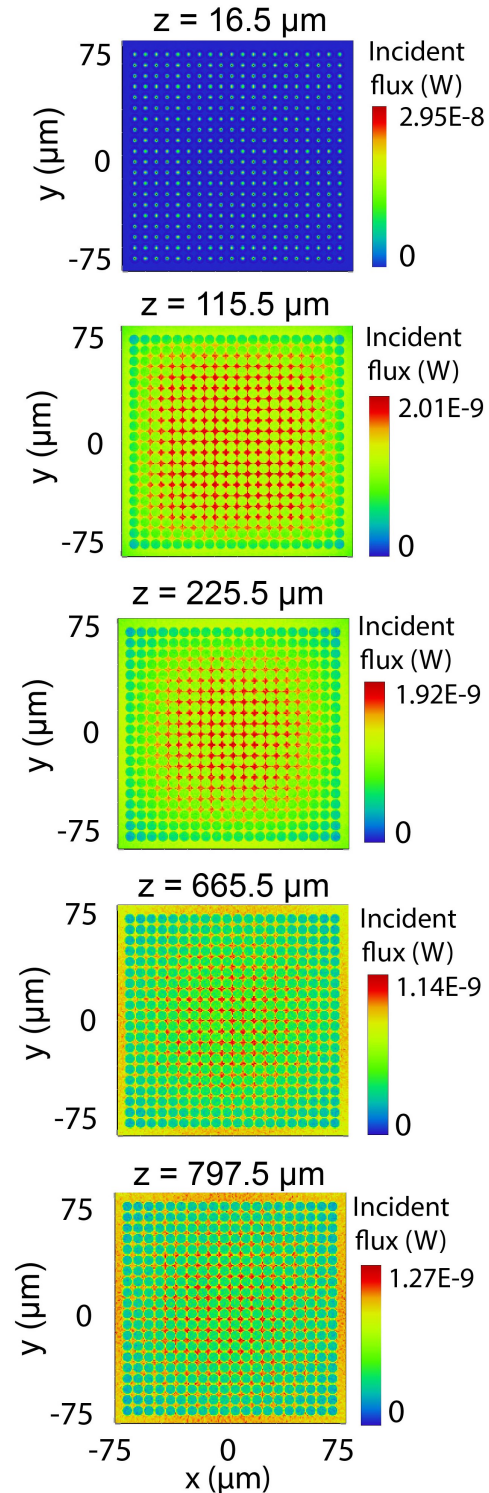


Figure 4: Top view intensity profile under (a) MLR and (b) MLA at the horizontal plane with the distance of $16.5 \mu\text{m}$, $115.5 \mu\text{m}$, $225.5 \mu\text{m}$, $665.5 \mu\text{m}$, and $797.5 \mu\text{m}$ away from the substrate surface.

308 The top view intensity profiles of surface MLs in Figure 4 (a-b) exhibit the distribution
309 of irradiance at the horizontal plane with certain depths. At the depth of $16.5 \mu\text{m}$ which
310 is close to the focal distances of MLA, the maximum incident flux value under MLA is the
311 highest, reaching $2.95 \times 10^{-8} \text{ W}$. The number of the spots with the highest value is 400 on
312 the horizontal plane with an area of $2.25 \times 10^{-2} \text{ mm}^2$. In comparison, the highest maximum
313 incident flux value under MLR is $2.26 \times 10^{-7} \text{ W}$ located at the depth of $225.5 \mu\text{m}$. However,
314 only two spots reach 2.26×10^{-7} on the horizontal plane under random MLs within the
315 same area. Therefore, the maximum total incident flux over the horizontal plane of MLA is
316 around 26 times larger than that of MLR.

317 When the depth increases, the maximum incident flux value under MLA significantly
318 drops, while the value under MLR first increases and then gradually diminishes. As the
319 depth changes from $16.5 \mu\text{m}$ to $797.5 \mu\text{m}$, the maximum flux value under MLA decreases by
320 56%, while the value under MLR increases by 3.6 times. The variation of focal distances of
321 MLR avoids the sharp decay of irradiation intensity along the Z direction but also causes a
322 lower maximum total incident flux. In summary, the uniformity of focal distances of MLA
323 can reach a maximum flux, higher than MLR, but the decay irradiation intensity along the
324 Z axis is much more rapid.

325 **Free radicals from MLs**

326 Based on the spectra obtained by ESR (Figure 5), no obvious signals can be observed when
327 neither ZnO nor surface MLs is used in the light treatment. Under both visible LED light
328 and simulated solar light, a similar curve shape is observed if ZnO is added to the system.
329 As described in the literature,⁷⁰ the spectrum indicates that $\cdot\text{OH}$ free radicals form with
330 the presence of ZnO. The formation of $\cdot\text{OH}$ accelerates the degradation of pollutants. When
331 MLA is applied together with ZnO, the signals of free radicals become stronger under both
332 visible LED light and simulated solar light. Therefore, it is possible that more free radicals are
333 generated by utilizing MLA. Consequently, more free radicals could cause higher degradation

334 efficiency (η).⁷²

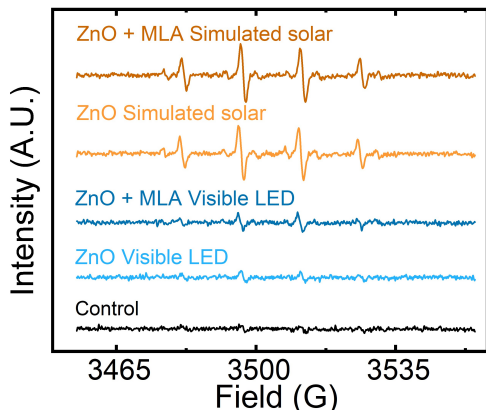


Figure 5: Electron spinning resonance (EPR) spectra under different conditions after light treatment of 30 min. (The black curve is for the condition without ZnO particles and surface MLs. The light blue curve represents the treatment with only ZnO particles, while the dark blue curve is for both ZnO and MLA under a visible LED lamp. The light orange curve is for the conditions with only ZnO particles, while the dark orange curve is for both ZnO and MLA under simulated solar light.)

335 Stronger signals of free radicals observed in the system with MLA could be attributed to
336 the higher light intensity at the focal points of MLs. Based on the second law of photochem-
337 istry,^{73,74} higher light intensity leads to a higher concentration of reactive species, such as
338 hydroxyl free radicals in the MLs-enhanced photocatalytic system.^{75,76} The light intensity
339 at focal points of surface MLs increases by several times as shown by the optical simulation
340 results (Figure 4). A higher concentration of active species in the MLs-induced system is
341 confirmed by ESR characterization in our previous work.⁵⁷ Similar to the photolysis system
342 without catalysis, the ESR spectra in Figure 5 suggested that the photodegradation with
343 ZnO as the catalyst could also be accelerated, due to the larger amount of free radicals from
344 the focusing effect of surface MLs.

345 The increase in the concentration of free radicals is the consequence of the stronger local
346 irradiance intensity in the presence of surface MLs. But the types of free radicals are not
347 expected different from the situation without MLs, as the types are only determined by the
348 light source and the type of photocatalyst. TiO_2 used in our experiments is a commercial-
349 ized photocatalyst that has been widely studied.^{77,78} According to ESR results reported in

350 the literature, we could conclude that hydroxyl free radicals form when TiO_2 acts as the
351 photocatalyst, which promotes the degradation of organic pollutants.

352 **Influence of catalyst concentration on the efficiency of photocat-** 353 **alytic degradation under visible light**

354 The absorbance curves of the solutions containing different pollutants before and after light
355 treatment are plotted in Figure 6. For the four pollutants treated under a visible LED lamp,
356 slight enhancement can be observed by only applying surface MLs. By comparing the two
357 types of surface MLs, MLA performs better than MLR since the decrease of absorbance peak
358 is more obvious.

359 As shown in the second column of the plots in Figure 6, the reduction in absorbance values
360 of all pollutants in the presence of ZnO particles improved. Such improvement becomes
361 larger when we increase the initial concentration of ZnO. By combining surface MLs with
362 ZnO particles, the absorbance peaks of pollutants further decrease. In the presence of ZnO,
363 more reduction of absorbance is also observed with MLA compared with MLR, indicating
364 the higher removal rates of pollutants with MLA.

365 The photodegradation efficiency of all pollutants under the visible LED light is plot-
366 ted over the concentration of ZnO in Figure 7 (a). As the concentration of ZnO particles
367 increases, η of all four pollutants is enhanced. However, the enhancement of η by adding
368 dispersed ZnO particles into the solutions differs with the type of pollutants. For the pho-
369 todegradation of MO with ZnO, η after the irradiation of 1 h is improved by 59.2% when the
370 ZnO concentration increases from 5 mg/L to 100 mg/L. For the other three pollutants, the
371 change of η after enhancing ZnO concentration from 5 mg/L to 100 mg/L is much smaller
372 than that of MO, which is 5.7% for NFX, 2.9% for SFD, and 2.3% for SMX. The pollutant
373 that is more difficult to degrade, which is SMX, has the least improvement when increasing
374 the concentration of ZnO. The different degradation mechanisms among the pollutants may
375 lead to the varied effectiveness of ZnO. Much higher η efficiency of MO degradation is pos-

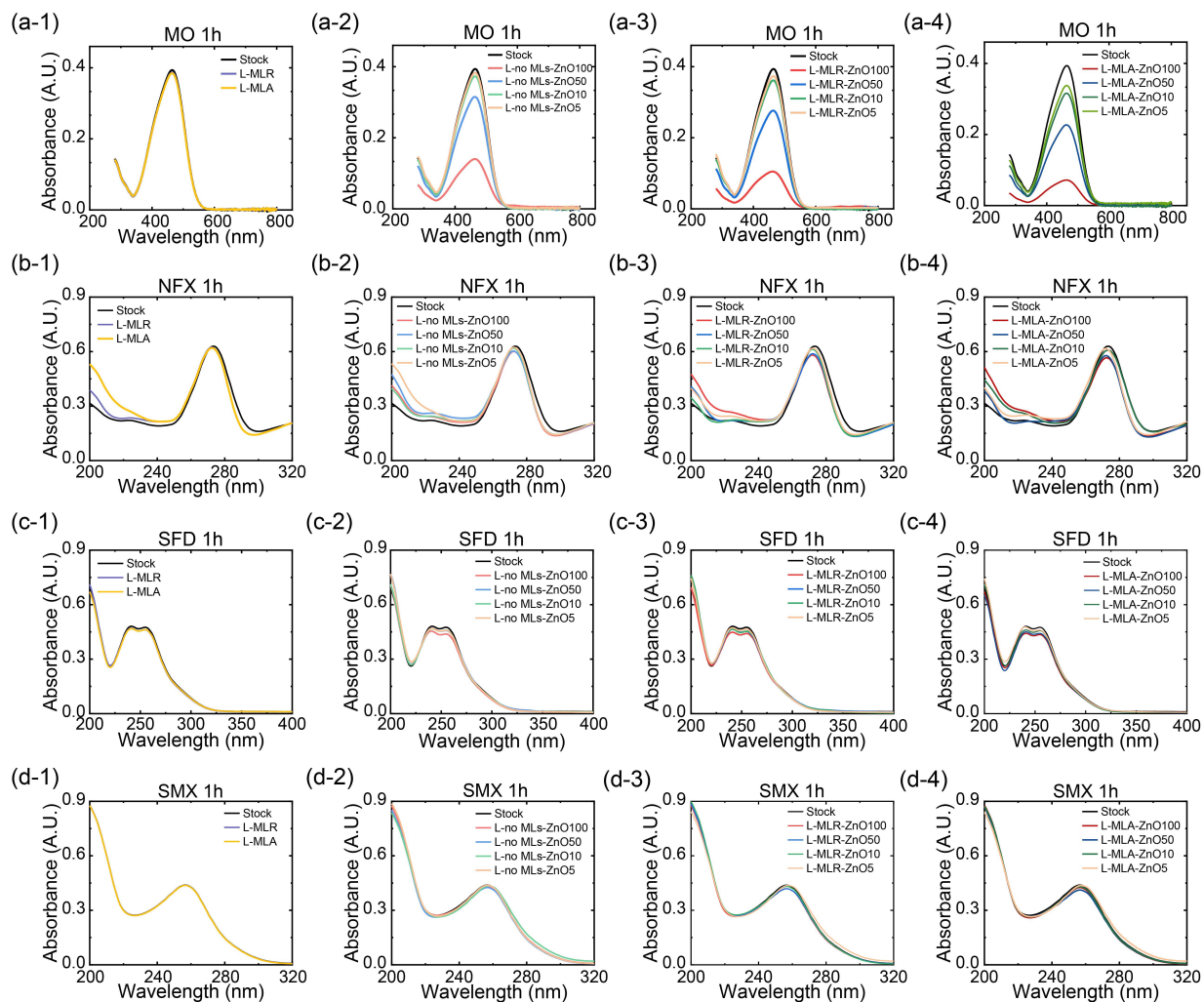


Figure 6: Representative absorbance spectra of pollutants (MO in (a-1) to (a-4), NFX in (b-1) to (b-4), SFD in (c-1) to (c-4), and SMX in (d-1) to (d-4)) with surface MLs and ZnO (under visible LED) after light treatment with 1 h.

376 sibly related to the sensitization mechanism for azo dyes. Charges are produced as the MO
377 molecules are excited under irradiance and then injected in photocatalysts and oxidized dye
378 for subsequent degradation.^{79,80} In contrast, the sensitization mechanism does not apply to
379 other tree organic compounds, including NFX, SFD, and SMX, since they are transparent
380 to the irradiation wavelengths. Regardless of the details in photodegradation mechanisms
381 for those organic contaminants, the enhancement in η is achieved for all of them by adding
382 ZnO.

383 Comparing with the situation only implementing ZnO or only surface MLs, the condition
384 with both MLs and ZnO shows higher η , indicating the synergistic effect in the surface MLs-
385 enhanced photocatalytic system. By applying surface MLs in the photocatalytic degradation
386 process with ZnO as the catalyst, the distinguished enhancement of η can be confirmed in all
387 four pollutants. The variance in the enhancement of η resulted not only from using surface
388 MLs but also from the increase in ZnO concentration, which is similar to the situation only
389 with adding ZnO in the reaction systems. The photocatalytic degradation exhibited higher
390 η with MLA compared with that using MLR. The possible reason for the more outstanding
391 effect of MLA is the more efficient irradiation redistribution based on the highly-ordered
392 structure in MLA, which is also demonstrated in the optical simulations.⁸¹

393 The enhancement factor for the MLs-enhanced photodegradation using ZnO as the cat-
394 alyst is calculated with equation (4). As shown in Figure 7 (e-h), the enhancement factor
395 becomes lower at higher ZnO concentrations. The amount of active species is the key factor
396 determining the rate of photodegradation. In the photodegradation enhanced by ZnO and
397 surface MLs, the number of active species is up to the dosage of ZnO and the number of hot
398 spots created by MLs.^{42,82} The total number of active species (N_{total}) can be estimated using
399 Equation (5). In the equation, $N_{catalyst}$ is the number of active species generated due to the
400 excitation of ZnO, and N_{MLs} is the number of active species attributed to the focus effect
401 of MLs. The photocatalytic degradation efficiency is dependent on the number of active
402 species in the system. Therefore, the enhancement factor with MLs is positively related to

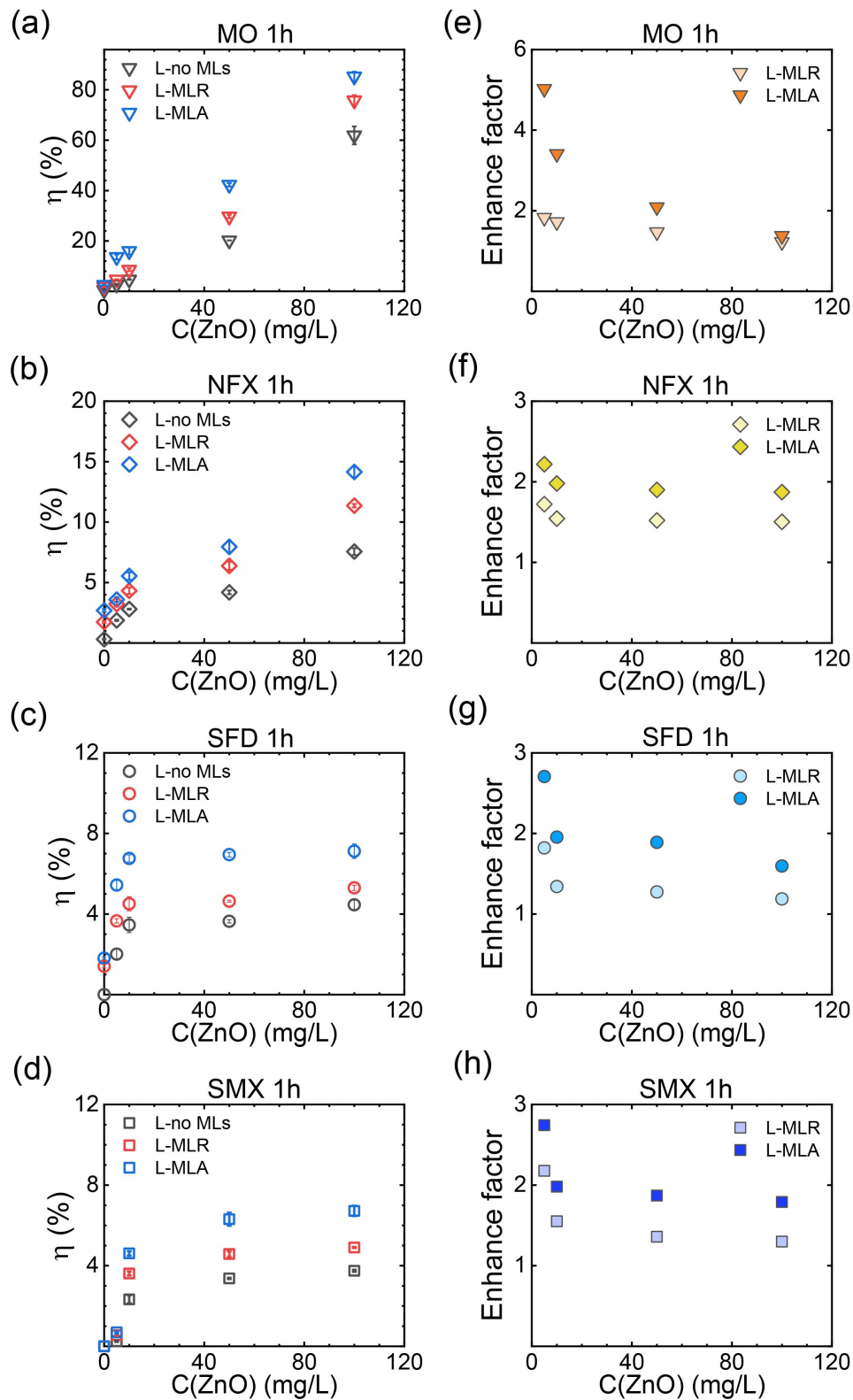


Figure 7: Photodegradation efficiency of (a) MO, (b) NFX, (c) SFD, (d) SMX using surface MLs and ZnO with different concentration (under visible LED). Enhancement of photodegradation efficiency of (e) MO, (f) NFX, (g) SFD, (h) SMX by using surface MLs

403 the ratio of N_{MLs} and $N_{catalyst}$ in Equation (6). With an increase in the concentration of
404 ZnO, $N_{catalyst}$ also increases while N_{MLs} is fixed, therefore, the enhancement factor drops
405 down.

$$N_{total} = N_{catalyst} + N_{MLs} \quad (5)$$

$$f \sim \frac{N_{total}}{N_{catalyst}} = 1 + \frac{N_{MLs}}{N_{catalyst}} \quad (6)$$

406 The enhancement factor in η of ZnO-photocatalyzed degradation by surface MLs is also
407 monitored with the elongated irradiation time of light treatment. The enhancement factor
408 for the four organic pollutants is plotted with the irradiation time in Figure 8. For MO
409 and SMX, the factor becomes smaller when the irradiation time increases from 1 h to 2 h.
410 Reversely, the factor grows in the photocatalytic degradation of NFX and SFD during a
411 longer treatment time. The difference in the enhancement factor not only is due to the type
412 of pollutants but is also related to the properties of MLs. The enhancement factor obtained
413 by MLR shows less change than that by MLA after the longer irradiation time.

414 **General enhancement of photocatalytic degradation with surface** 415 **MLs under visible light**

416 The effectiveness of surface MLs is verified by using a different catalyst in the photocatalytic
417 degradation process. As shown in Figure 9 (a-d), more decrease in absorbance peaks is
418 presented when TiO_2 is used as the catalyst compared to that without a catalyst. When
419 combining TiO_2 with surface MLs, more organic pollutants are degraded than those in the
420 treatment with only TiO_2 . After the same light treatment process, the MLA-enhanced
421 photocatalytic degradation with TiO_2 has the most decrease in absorbance peak values.

422 The η values of all pollutants after the irradiation of 1 h with only TiO_2 or with both TiO_2
423 and MLs are displayed in Figure 9 (e). The η values of all four pollutants have been further

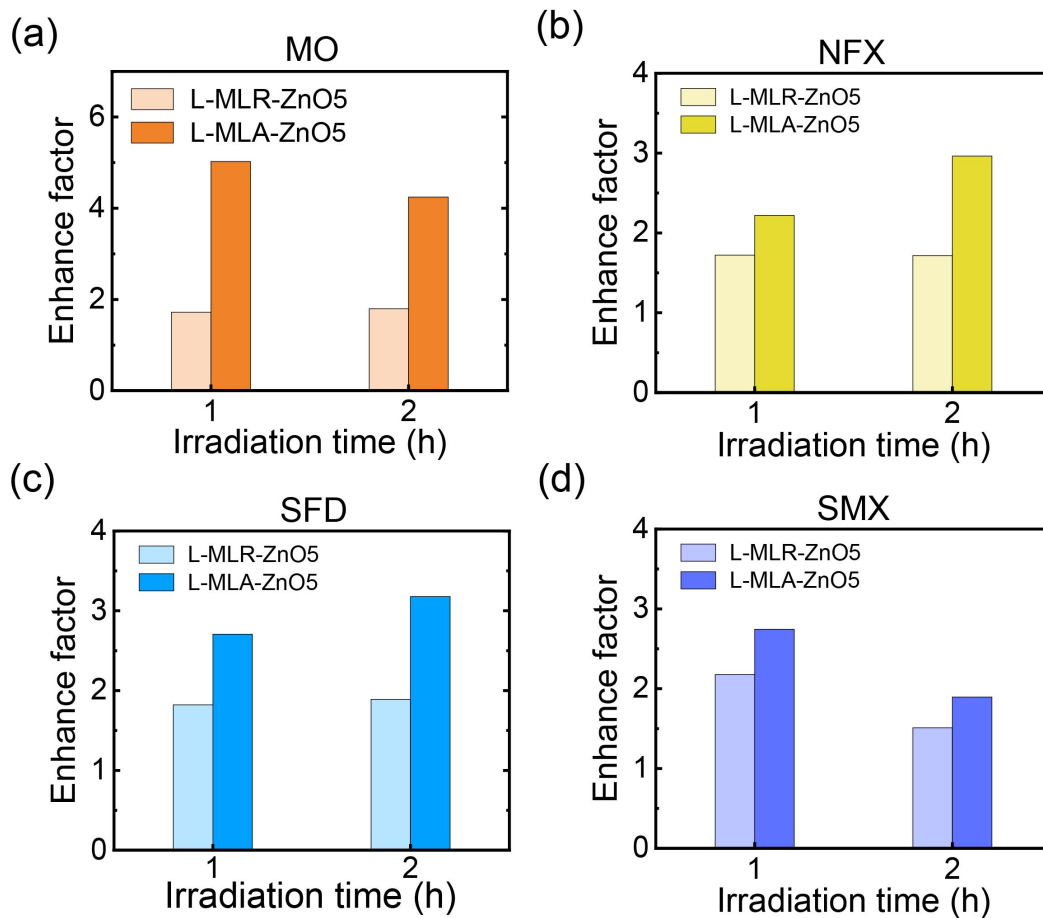


Figure 8: Enhancement factor of ZnO-photocatalyzed degradation efficiency of (a) MO, (b) NFX, (c) SFD, (d) SMX with surface MLs after irradiation time of 1 h and 2 h.

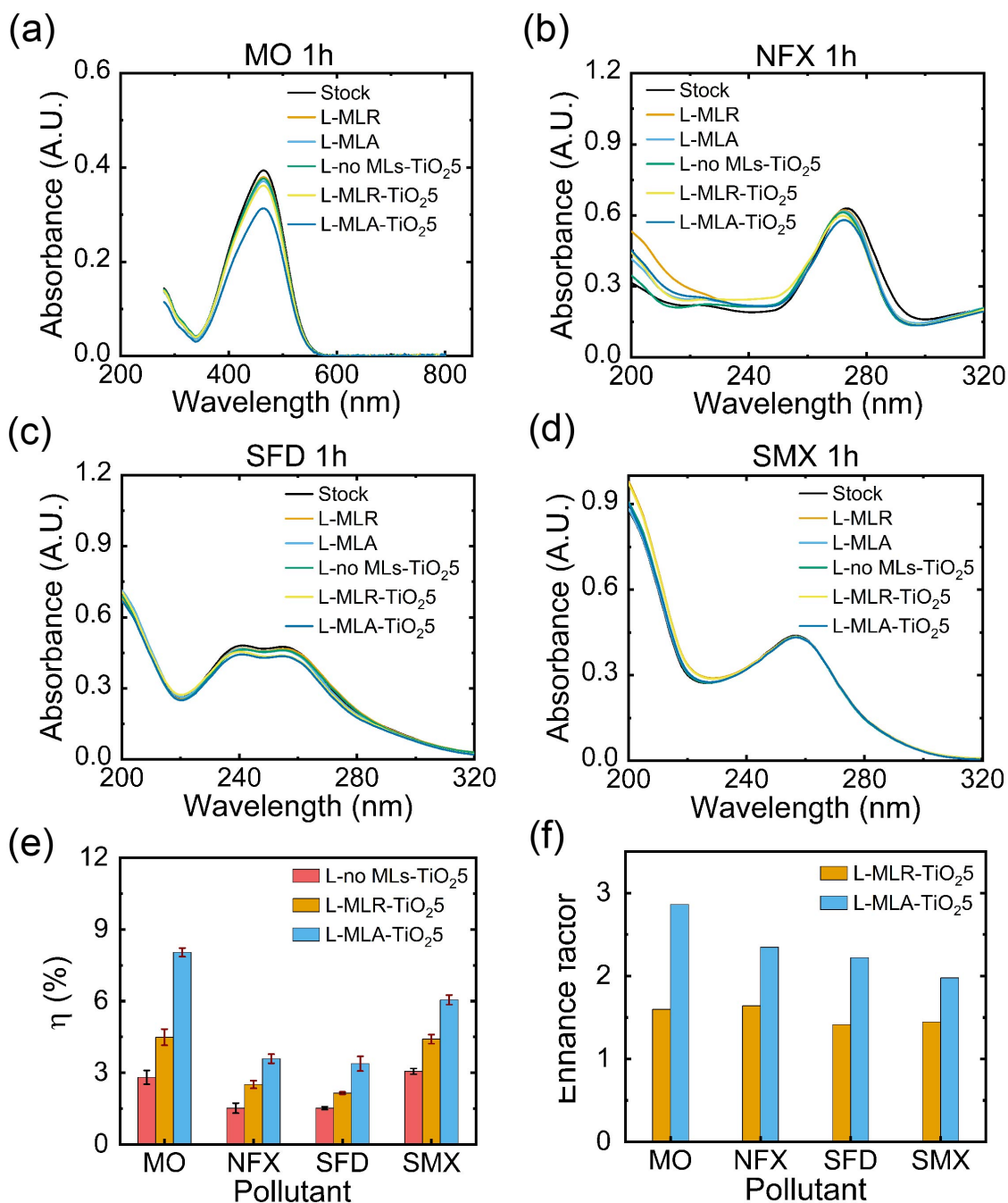


Figure 9: Representative absorbance curves of (a) MO, (b) NFX, (c) SFD, (d) SMX after the light treatment under the visible LED lamp for 1 h. (e) Photodegradation efficiency and (f) enhancement factor of TiO_2 -photocatalytic degradation efficiency of pollutants with surface MLs after irradiation time of 1 h.

424 improved after applying MLs in the photocatalytic degradation with TiO_2 . Moreover, MLA
425 shows more enhancement compared to MLR. The enhancement factor by using MLR and
426 MLA are shown in Figure 9 (f). The effect of surface MLs on the degradation catalyzed by
427 TiO_2 is similar to that catalyzed by ZnO. Therefore, surface MLs accelerate photocatalytic
428 degradation, regardless of the types of catalysts.

429 **MLs-enhanced photocatalytic degradation under simulated solar** 430 **light**

431 The representative absorbance spectra of SMX solution after the irradiation under different
432 conditions are shown in Figure 10 (a-d). By comparing Figure 10 (a) and (c), it is found
433 that the absorbance peak drops faster when the concentration of ZnO increases. As shown
434 in Figure 10 (a) and (b), the decrease of absorbance peak value is higher when MLA is used
435 in the light treatment. Such difference is also displayed in Figure 10 (c) and (d), where the
436 concentration of ZnO changes to 10 mg/L.

437 The η values of all conditions presented in Figure 10 (a-d) are plotted in Figure 10 (e).
438 For the concentration of ZnO equal to 100 mg/L, η reaches 72.4% within 3 h when both
439 MLA and ZnO were used. To achieve a similar η with the ZnO concentration of 10 mg/L,
440 around 5 h is required in the presence of MLA. The η under the simulated solar light is
441 higher than that under the visible LED light due to the difference in light intensities and
442 wavelength range.

443 The degradation efficiency of SMX with MLA is higher than that without MLA under
444 the simulated light, which is the same phenomenon under visible light. The enhancement
445 factors by MLA with two concentrations of ZnO under the simulated solar light are plotted
446 with the irradiation time in Figure 10 (f). When the concentration of ZnO is 100 mg/L, the
447 enhancement factor fluctuates around 1.2 as the irradiation time changes from 1 h to 3 h.
448 For the photocatalytic degradation with a ZnO concentration of 10 mg/L, the enhancement
449 factor by MLA is higher than that with 100 mg/L of ZnO. However, the factor drops from

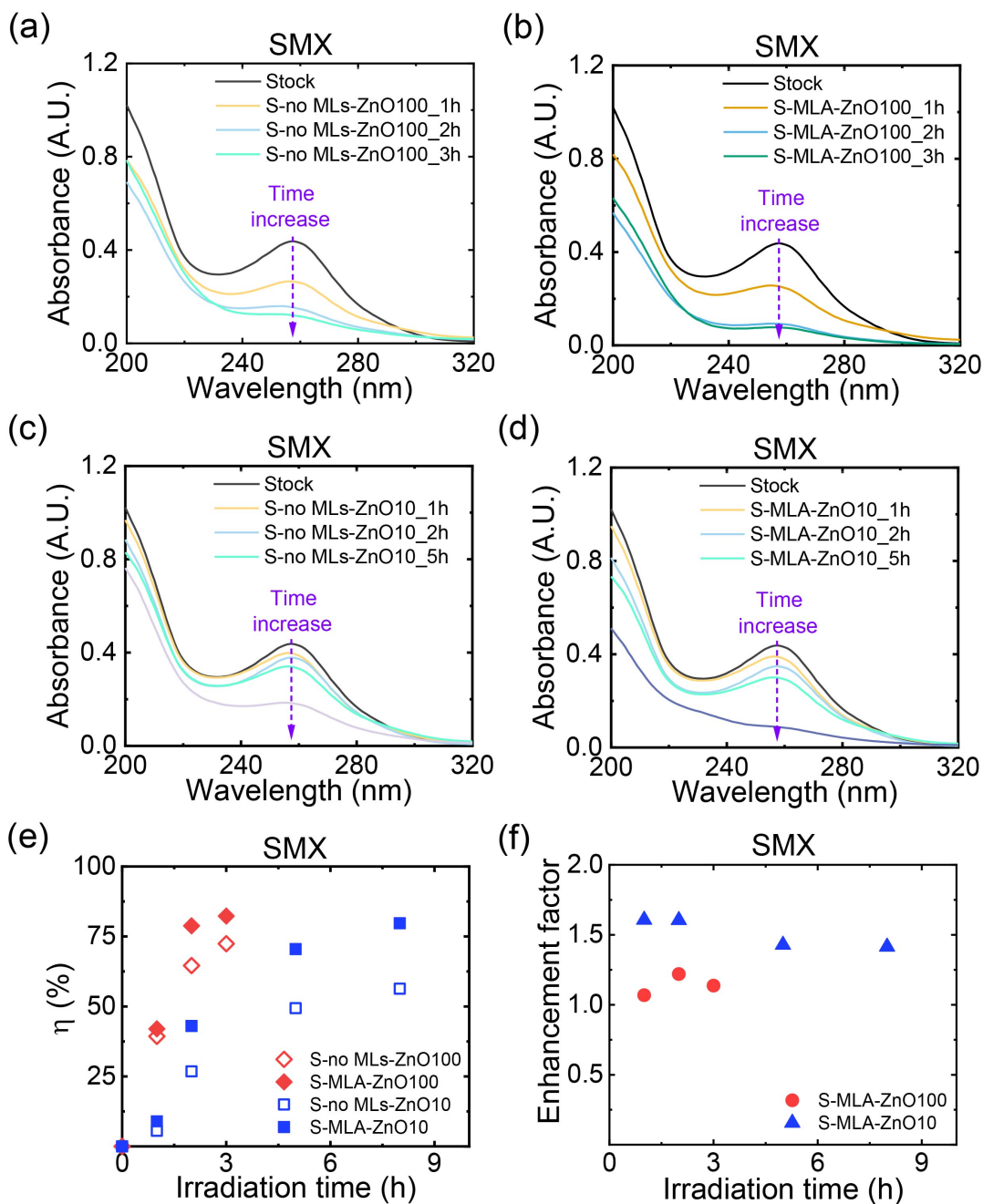


Figure 10: Representative absorbance curve of SMX solution after the light treatment with (a) only ZnO particles with a concentration of 100 mg/L (b) both ZnO with a concentration of 100 mg/L and MLA (c) only ZnO particles with a concentration of 10 mg/L (d) both ZnO with a concentration of 10 mg/L and MLA under the simulated solar light. (e) Photodegradation efficiency and (f) enhancement factor of SMX under different conditions.

450 1.6 to 1.4 as the irradiation time increases from 1 h to 8 h. The results under the simulated
 451 solar light reveal that the ordered spatial arrangement of MLs is optimal for photocatalytic
 452 degradation when the light source is closer to real solar light. The higher enhancement factor
 453 under the lower concentration of ZnO further validates our assumption shown in Equation
 454 (6) under simulated solar light.

455 The η of MLs-enhanced photocatalytic degradation of SMX is positively correlated with
 456 the intensity of simulated solar light in the range from 0.3 Sun to 1 Sun (Figure 11 (a-
 b)). As the irradiation time increases from 1 h to 2 h, the enhancement of η by improving

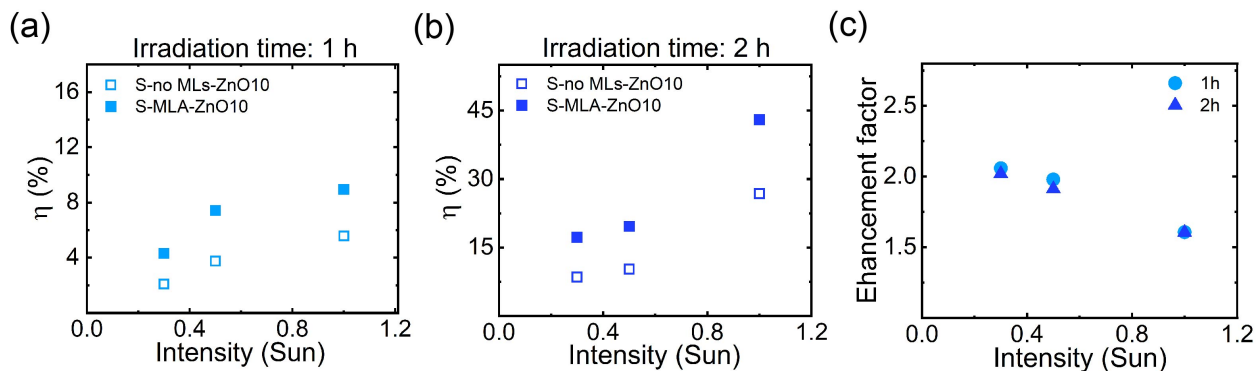


Figure 11: Photodegradation efficiency of SMX after the irradiation for (a) 1 h and (b) 2 h under the irradiation of the simulated solar light with different intensities (c) The enhancement factor of η by using MLA during the irradiation for 1 h and 2 h

457

458 the intensity of light is different. As the light intensity increases from 0.3 Sun to 1 Sun,
 459 the η increases from 2.1% to 5.6% with only ZnO after the irradiation of 1 h, while the
 460 η is enhanced from 4.3% to 9.0% by using ZnO combined with MLA. (Figure 11 (a)) The
 461 enhancement in η becomes larger when the irradiation time increases to 2 h based on Figure
 462 11 (b).

463 In addition, the η of SMX with both of MLA and ZnO is always higher than that with
 464 only ZnO under varying light intensities. The enhancement factor obtained by using MLA
 465 is shown in Figure 11 (c). Under irradiation with the same light intensity, the change of the
 466 enhancement factor after adding the irradiation time from 1 h to 2 h is less than 0.6. The
 467 influence of irradiation on the performance of MLA is negligible in the first two hours of

468 photodegradation of SMX. The enhancement factor drops down when the intensity becomes
469 higher, showing that surface MLs perform better under irradiation with low light intensity.

470 MLs-enhanced photocatalytic degradation in a glass container

471 The MLs-enhanced photocatalytic degradation can be conducted in the MLs-decorated glass
472 vials. As demonstrated in Figure 12 (a), the glass vial keeps transparent with surface MLs
473 immobilized on the inner wall. In the microscopic image (Figure 12 (b)), surface MLs on
474 the vial gave various sizes and random spatial distributions because of the homogeneous
475 hydrophobic coating on the inner surface of the vial. The diameter of MLs displayed in the
476 picture is from 1.40 μm to 310 μm . The surface coverage rate of the MLs is around 50%.

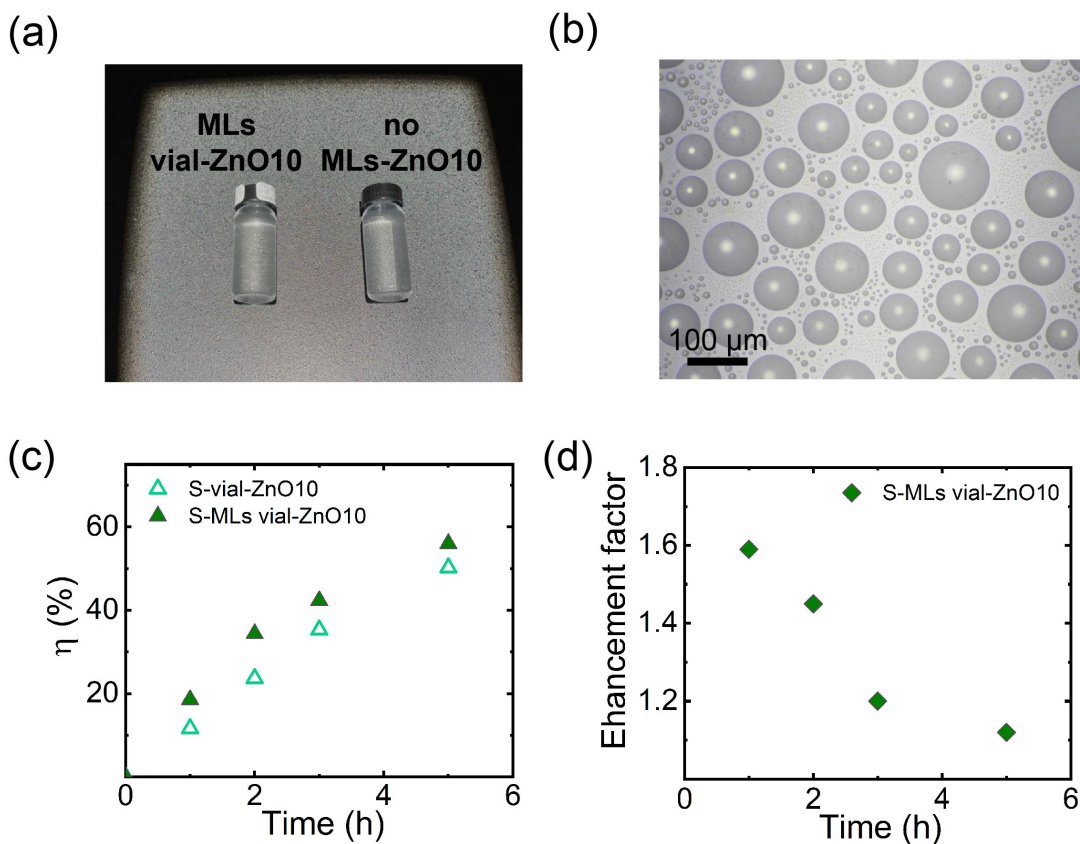


Figure 12: (a) Experimental set-up of ZnO-photocatalyzed degradation of SMX solution with the MLs-decorated vial ($C(\text{ZnO})=10$ mg/L, $C(\text{SMX})=5$ mg/L, $\text{pH}=7.0$) (b) The optical image of the MLs on the inner wall of a glass vial (c) Photodegradation efficiency of SMX with ZnO in a bare glass vial and an MLs-decorated vial (d) Enhancement factor of ZnO-photocatalyzed degradation with the MLs-decorated vial

477 The application of MLs-decorated vials can also enhance the η of degradation. As shown
478 in Figure 12 (c), the η of degradation with MLA obtained from UV Vis spectra (supporting
479 information, Figure S3) is always higher than that using only ZnO. Under the irradiation
480 of simulated solar light (1 Sun), the η of SMX with ZnO (10 mg/L) reaches 50.2% after
481 five hours of light treatment, while the value is further improved to 56.0% after using the
482 MLs-decorated vial. As demonstrated in Figure 12 (d), the enhancement factor by using
483 MLs-decorated vials is 1.60 after the irradiation for 1 h and then continuously decreases
484 with the irradiation time.

485 The degradation of SMX is significantly influenced by the concentration of SMX. When
486 the concentration of SMX is less than 5 mg/L, a lower concentration of SMX results in a
487 lower degradation rate.⁸³ The higher degradation rate with the existence of surface MLs
488 directly leads to a lower concentration of SMX after irradiation. Therefore, the degradation
489 rate of SMX with surface MLs drops faster than the process happening in the bare vial. As
490 a consequence, the enhancement factor with MLs-decorated vials will decrease with time.

491 **Effect of water matrix on MLs-enhanced photodegradation**

492 The photocatalytic degradation of SMX with ZnO can be enhanced with surface MLs not
493 only in ultra-pure water but also in synthetic river water and real river water. The photo in
494 Figure 13 (a) displays the collection point of the river water. By comparing the transmittance
495 curves of different water matrices (Figure 13 (b)), we find that the transparency of synthetic
496 water and river water is less than that of river water, especially in the wavelength ranging
497 from 200 nm to 500 nm.

498 As displayed in Figure 13 (c), the η of SMX with both MLR and MLA is improved
499 compared with that with only ZnO. Similar to the results observed in pure water, MLA
500 has better performance than MLR in accelerating the photodegradation of SMX. The η
501 with the same type of MLs and irradiation time in the synthetic water is lower than that
502 achieved in the ultra-pure water (Figure 10 (e)). Compared with the enhancement factor

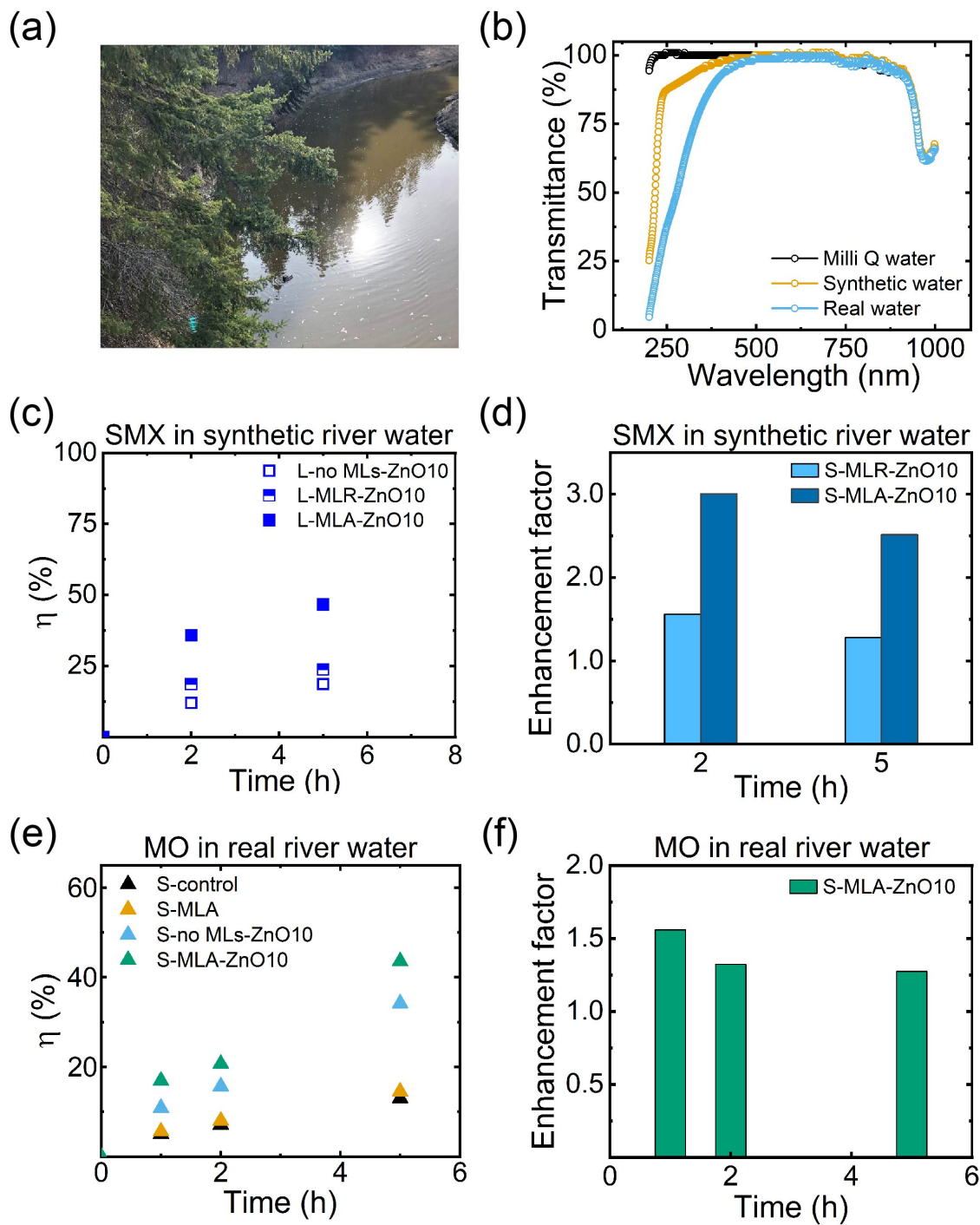


Figure 13: (a) A photo of the real river water collection site (b) Transmittance curves of three types of water matrices (c) Photodegradation efficiency of SMX in simulated water under simulated solar light (d) Enhancement factor of photocatalytic photodegradation efficiency of SMX achieved by MLR and MLA during 2 h and 5 h of irradiation. (e) Photodegradation efficiency of MO in the real river water under simulated solar light (f) Enhancement factor of photocatalytic photodegradation efficiency of MO obtained by MLA during 1 h, 2 h, and 5 h of irradiation.

503 with surface MLs in ultra-pure water during the same irradiation time, the enhancement
504 factor in synthetic river water is higher. For example, the enhancement factor of MLR is
505 1.61 and 1.43 after 2 h and 5 h of irradiation, respectively. When using MLA, the factor is
506 3.0 for 2 h and 2.5 for 5 h (Figure 13 (d)).

507 The enhancement of photocatalytic degradation is also observed when using real river
508 water as the matrix. The photodegradation efficiency of MO in river water and the enhance-
509 ment factor of η over the irradiation time are plotted in Figure 13 (e) and (f), respectively.
510 Without utilizing ZnO, around 14% enhancement is achieved by MLA after 5 h of irradiation.
511 Compared with the condition without the catalyst and surface MLs, the degradation
512 efficiency of MO is enhanced by a maximum of 163% with only ZnO after 5 h of irradiation.
513 By setting MLA on the top of the light treatment chamber, the photocatalytic η of MO
514 is further improved under the same irradiation condition, which is 235% higher than the
515 control group and 27% higher than the group only with catalyst.

516 The difference in η and the enhancement factor after changing the water matrix into syn-
517 thetic river water or real river water can be attributed to the variation in the transmittance
518 of water. The transmittance of the synthetic water in the range between 200 nm and 500
519 nm drops as displayed in Figure 13 (b), while the decrease in transmittance of river water is
520 even sharper. The decrease in the transmittance is possibly caused by more light absorption
521 of the synthetic river water and real river water. As a consequence, the irradiation intensity
522 in synthetic river water and river water should be lower than that in ultra-pure water, thus
523 the enhancement of η by surface MLs is higher (as displayed in Figure 11 (c)).

524 Conclusions

525 In summary, our work demonstrates the microlenses(MLs)-enhanced photocatalytic degra-
526 dation efficiency of micropollutants in water. More free radicals generated in the presence
527 of surface MLs contribute to higher degradation efficiency. The enhancement is generally

528 observed for all four targeted organic contaminants by using two kinds of photocatalysts.
529 The microlens array is more effective than random microlenses in the photodegradation of
530 all involved pollutants, which is attributed to the more effective redistribution of the irra-
531 diation energy. The performance of surface MLs, represented by an enhancement factor,
532 varies with pollutants because of the difference in degradation mechanisms. Additionally,
533 the enhancement in the η of photocatalytic degradation is higher at a lower concentration
534 of the photocatalyst or under irradiation with lower intensity. Therefore, the results suggest
535 that surface MLs have the potential for applications where the excitation of photocatalysts
536 is suppressed. The feasibility of surface MLs in improving decontamination is also verified
537 in synthetic river water and a real river water matrix. In the next stage, surface MLs may
538 be tested in the light treatment of water samples containing multiple contaminants.

539 **Supporting Information Available**

540 Supplementary data to this article can be found in the document attached. Additional data
541 include.

- 542 • Filename: Supplementary information.docx

543 **Acknowledgement**

544 The authors acknowledge the support from Canada First Research Excellence Fund as part
545 of the University of Alberta's Future Energy System research initiative and the technical
546 assistance from the Institute for Oil Sands Innovation (IOSI) at the University of Alberta.
547 This research was undertaken, in part, thanks to funding from the Canada Research Chairs
548 Program and Canada Foundation for Innovation. This work was also supported by a Natural
549 Sciences and Engineering Research Council of Canada (NSERC) Senior Industrial Research
550 Chair (IRC) in Oil Sands Tailings Water Treatment through the support of Canada's Oil

551 Sands Innovation Alliance (COSIA), Syncrude Canada Ltd., Suncor Energy Inc., Canadian
552 Natural Resources Ltd., Imperial Oil Resources, Teck Resources Limited, EPCOR Water
553 Services, Alberta Innovates, and Alberta Environment and Parks. MGED appreciates fund-
554 ing from NSERC Discovery Grant programs.

References

- (1) Suara, M. A.; Ganiyu, S. O.; Paul, S.; Stafford, J. L.; El-Din, M. G. Solar-activated zinc oxide photocatalytic treatment of real oil sands process water: Effect of treatment parameters on naphthenic acids, polyaromatic hydrocarbons and acute toxicity removal. *Science of The Total Environment* **2022**, *819*, 153029.
- (2) Arnold, D. R.; Baird, N.; Bolton, J. R. *Photochemistry: an introduction*; Academic Press, 2014.
- (3) Li, F.; Zhuang, J.; Jiang, G.; Tang, H.; Xia, A.; Jiang, L.; Song, Y.; Li, Y.; Zhu, D. A Rewritable Optical Data Storage Material System by [2+ 2] Photocycloreversion-Photocycloaddition. *Chemistry of Materials* **2008**, *20*, 1194–1196.
- (4) Li, N.-Y.; Chen, J.-M.; Tang, X.-Y.; Zhang, G.-P.; Liu, D. Reversible single-crystal-to-single-crystal conversion of a photoreactive coordination network for rewritable optical memory storage. *Chemical Communications* **2020**, *56*, 1984–1987.
- (5) Pradhan, N. R.; Ludwig, J.; Lu, Z.; Rhodes, D.; Bishop, M. M.; Thirunavukkuarasu, K.; McGill, S. A.; Smirnov, D.; Balicas, L. High photoresponsivity and short photoresponse times in few-layered WSe₂ transistors. *ACS applied materials & interfaces* **2015**, *7*, 12080–12088.
- (6) Kimoto, A.; Cho, J.-S.; Ito, K.; Aoki, D.; Miyake, T.; Yamamoto, K. Novel Hole-Transport Material for Efficient Polymer Light-Emitting Diodes by Photoreaction. *Macromolecular rapid communications* **2005**, *26*, 597–601.
- (7) Zhou, Y.; Zhang, H.-Y.; Zhang, Z.-Y.; Liu, Y. Tunable luminescent lanthanide supramolecular assembly based on photoreaction of anthracene. *Journal of the American Chemical Society* **2017**, *139*, 7168–7171.

- 578 (8) Corrigan, N.; Yeow, J.; Judzewitsch, P.; Xu, J.; Boyer, C. Seeing the light: advancing
579 materials chemistry through photopolymerization. *Angewandte Chemie International*
580 *Edition* **2019**, *58*, 5170–5189.
- 581 (9) Bagheri, A.; Jin, J. Photopolymerization in 3D printing. *ACS Applied Polymer Mate-*
582 *rials* **2019**, *1*, 593–611.
- 583 (10) Kumar, A.; Khan, M.; He, J.; Lo, I. M. Recent developments and challenges in practical
584 application of visible–light–driven TiO₂–based heterojunctions for PPCP degradation:
585 a critical review. *Water research* **2020**, *170*, 115356.
- 586 (11) Luo, Z.; Meng, L.; How, Z. T.; Chelme-Ayala, P.; Yang, L.; Benally, C.; El-Din, M. G.
587 Treatment of oil sands process water by the ferric citrate under visible light irradiation.
588 *Chemical Engineering Journal* **2022**, *429*, 132419.
- 589 (12) Edzwald, J.; Association, A. W. W., et al. *Water quality & treatment: a handbook on*
590 *drinking water*; McGraw-Hill Education, 2011.
- 591 (13) Sommer, B.; Marino, A.; Solarte, Y.; Salas, M.; Dierolf, C.; Valiente, C.; Mora, D.;
592 Rechsteiner, R.; Setter, P.; Wirojanagud, W., et al. SODIS- an emerging water treat-
593 ment process. *AQUA(OXFORD)* **1997**, *46*, 127–137.
- 594 (14) Dejung, S.; Fuentes, I.; Almanza, G.; Jarro, R.; Navarro, L.; Arias, G.; Urquieta, E.;
595 Torrico, A.; Fenandez, W.; Iriarte, M., et al. Effect of solar water disinfection (SODIS)
596 on model microorganisms under improved and field SODIS conditions. *Journal of Water*
597 *Supply: Research and Technology—AQUA* **2007**, *56*, 245–256.
- 598 (15) Callao, M. P.; Larrechi, M. S. *Data Handling in Science and Technology*; Elsevier, 2015;
599 Vol. 29; pp 399–426.
- 600 (16) Chen, D.; Cheng, Y.; Zhou, N.; Chen, P.; Wang, Y.; Li, K.; Huo, S.; Cheng, P.; Peng, P.;

- 601 Zhang, R., et al. Photocatalytic degradation of organic pollutants using TiO₂-based
602 photocatalysts: A review. *Journal of Cleaner Production* **2020**, *268*, 121725.
- 603 (17) Bhatkhande, D. S.; Pangarkar, V. G.; Beenackers, A. A. C. M. Photocatalytic degra-
604 dation for environmental applications—a review. *Journal of Chemical Technology &*
605 *Biotechnology: International Research in Process, Environmental & Clean Technology*
606 **2002**, *77*, 102–116.
- 607 (18) Dong, H.; Zeng, G.; Tang, L.; Fan, C.; Zhang, C.; He, X.; He, Y. An overview on
608 limitations of TiO₂-based particles for photocatalytic degradation of organic pollutants
609 and the corresponding countermeasures. *Water research* **2015**, *79*, 128–146.
- 610 (19) Lee, K. M.; Lai, C. W.; Ngai, K. S.; Juan, J. C. Recent developments of zinc oxide
611 based photocatalyst in water treatment technology: a review. *Water research* **2016**,
612 *88*, 428–448.
- 613 (20) Rehman, S.; Ullah, R.; Butt, A.; Gohar, N. Strategies of making TiO₂ and ZnO visible
614 light active. *Journal of hazardous materials* **2009**, *170*, 560–569.
- 615 (21) Davis, K.; Yarbrough, R.; Froeschle, M.; White, J.; Rathnayake, H. Band gap en-
616 gineered zinc oxide nanostructures via a sol–gel synthesis of solvent driven shape-
617 controlled crystal growth. *RSC advances* **2019**, *9*, 14638–14648.
- 618 (22) Tang, Y.; Zhou, H.; Zhang, K.; Ding, J.; Fan, T.; Zhang, D. Visible-light-active ZnO via
619 oxygen vacancy manipulation for efficient formaldehyde photodegradation. *Chemical*
620 *Engineering Journal* **2015**, *262*, 260–267.
- 621 (23) Dette, C.; Pérez-Osorio, M. A.; Kley, C. S.; Punke, P.; Patrick, C. E.; Jacobson, P.;
622 Giustino, F.; Jung, S. J.; Kern, K. TiO₂ anatase with a bandgap in the visible region.
623 *Nano letters* **2014**, *14*, 6533–6538.

- 624 (24) Hotchandani, S.; Kamat, P. V. Photoelectrochemistry of semiconductor ZnO particu-
625 late films. *Journal of the Electrochemical Society* **1992**, *139*, 1630.
- 626 (25) Li, X.; Hu, Z.; Liu, J.; Li, D.; Zhang, X.; Chen, J.; Fang, J. Ga doped ZnO photonic
627 crystals with enhanced photocatalytic activity and its reaction mechanism. *Applied*
628 *Catalysis B: Environmental* **2016**, *195*, 29–38.
- 629 (26) Pitre, S. P.; Yoon, T. P.; Scaiano, J. C. Titanium dioxide visible light photocataly-
630 sis: surface association enables photocatalysis with visible light irradiation. *Chemical*
631 *Communications* **2017**, *53*, 4335–4338.
- 632 (27) Liu, J.; Zhao, H.; Wu, M.; Van der Schueren, B.; Li, Y.; Deparis, O.; Ye, J.; Ozin, G. A.;
633 Hasan, T.; Su, B.-L. Slow photons for photocatalysis and photovoltaics. *Advanced Ma-*
634 *terials* **2017**, *29*, 1605349.
- 635 (28) Diepens, M.; Gijssman, P. Influence of light intensity on the photodegradation of bisphe-
636 nol A polycarbonate. *Polymer Degradation and Stability* **2009**, *94*, 34–38.
- 637 (29) Tanveer, M.; Guyer, G. T. Solar assisted photo degradation of wastewater by com-
638 pound parabolic collectors: Review of design and operational parameters. *Renewable*
639 *and Sustainable Energy Reviews* **2013**, *24*, 534–543.
- 640 (30) Khaksar, A. M.; Nazif, S.; Taebi, A.; Shahghasemi, E. Treatment of phenol in petro-
641 chemical wastewater considering turbidity factor by backlight cascade photocatalytic
642 reactor. *Journal of photochemistry and photobiology A: chemistry* **2017**, *348*, 161–167.
- 643 (31) Vaghasiya, J. V.; Sonigara, K. K.; Suresh, L.; Panahandeh-Fard, M.; Soni, S. S.;
644 Tan, S. C. Efficient power generating devices utilizing low intensity indoor lights via
645 non-radiative energy transfer mechanism from organic ionic redox couples. *Nano Energy*
646 **2019**, *60*, 457–466.

- 647 (32) Kandy, M. M.; Gaikar, V. G. Enhanced photocatalytic reduction of CO₂ using
648 CdS/Mn₂O₃ nanocomposite photocatalysts on porous anodic alumina support with
649 solar concentrators. *Renewable Energy* **2019**, *139*, 915–923.
- 650 (33) Zhang, C.; Liu, N.; Ming, J.; Sharma, A.; Ma, Q.; Liu, Z.; Chen, G.; Yang, Y. De-
651 velopment of a novel solar energy controllable Linear fresnel photoreactor (LFP) for
652 high-efficiency photocatalytic wastewater treatment under actual weather. *Water Re-*
653 *search* **2022**, *208*, 117880.
- 654 (34) Nakano, M.; Nishiyama, Y.; Tanimoto, H.; Morimoto, T.; Kakiuchi, K. Remarkable
655 improvement of organic photoreaction efficiency in the flow microreactor by the slug
656 flow condition using water. *Organic Process Research & Development* **2016**, *20*, 1626–
657 1632.
- 658 (35) Li, W.; Wu, S.; Zhang, H.; Zhang, X.; Zhuang, J.; Hu, C.; Liu, Y.; Lei, B.; Ma, L.;
659 Wang, X. Enhanced biological photosynthetic efficiency using light-harvesting engineer-
660 ing with dual-emissive carbon dots. *Advanced Functional Materials* **2018**, *28*, 1804004.
- 661 (36) Zijffers, J.-W. F.; Salim, S.; Janssen, M.; Tramper, J.; Wijffels, R. H. Capturing sunlight
662 into a photobioreactor: Ray tracing simulations of the propagation of light from capture
663 to distribution into the reactor. *Chemical Engineering Journal* **2008**, *145*, 316–327.
- 664 (37) Daly, D. *Microlens arrays*; CRC Press, 2000.
- 665 (38) Commander, L.; Day, S.; Selviah, D. Variable focal length microlenses. *Optics commu-*
666 *nications* **2000**, *177*, 157–170.
- 667 (39) Seo, J.; Lee, L. P. Disposable integrated microfluidics with self-aligned planar mi-
668 crolenses. *Sensors and actuators B: Chemical* **2004**, *99*, 615–622.
- 669 (40) Dong, L.; Agarwal, A. K.; Beebe, D. J.; Jiang, H. Adaptive liquid microlenses activated
670 by stimuli-responsive hydrogels. *Nature* **2006**, *442*, 551–554.

- 671 (41) Lee, J. Y.; Hong, B. H.; Kim, W. Y.; Min, S. K.; Kim, Y.; Jouravlev, M. V.; Bose, R.;
672 Kim, K. S.; Hwang, I.-C.; Kaufman, L. J., et al. Near-field focusing and magnification
673 through self-assembled nanoscale spherical lenses. *Nature* **2009**, *460*, 498–501.
- 674 (42) Dyett, B.; Zhang, Q.; Xu, Q.; Wang, X.; Zhang, X. Extraordinary Focusing Effect of
675 Surface Nanolenses in Total Internal Reflection Mode. *ACS central science* **2018**, *4*,
676 1511–1519.
- 677 (43) Bao, Y.; Lee, W. J.; Seow, J. Z. Y.; Hara, H.; Liang, Y. N.; Feng, H.; Xu, J. Z.; Lim, T.-
678 T.; Hu, X. One-Step Block Copolymer Templated Synthesis of Bismuth Oxybromide
679 for Bisphenol A Degradation: An Extended Study from Photocatalysis to Chemical
680 Oxidation. *ACS ES&T Water* **2021**, *1*, 837–846.
- 681 (44) Wu, X.; Fang, C.; Xu, W.; Zhang, D. Bioinspired Compound Eyes for Diffused Light-
682 Harvesting Application. *ACS Applied Materials & Interfaces* **2022**,
- 683 (45) Huang, Y.; Qin, Y.; Tu, P.; Zhang, Q.; Zhao, M.; Yang, Z. High fill factor microlens
684 array fabrication using direct laser writing and its application in wavefront detection.
685 *Optics Letters* **2020**, *45*, 4460–4463.
- 686 (46) Hua, J.-G.; Ren, H.; Jia, A.; Tian, Z.-N.; Wang, L.; Juodkazis, S.; Chen, Q.-D.; Sun, H.-
687 B. Convex silica microlens arrays via femtosecond laser writing. *Optics letters* **2020**,
688 *45*, 636–639.
- 689 (47) Moore, S.; Gomez, J.; Lek, D.; You, B. H.; Kim, N.; Song, I.-H. Experimental study of
690 polymer microlens fabrication using partial-filling hot embossing technique. *Microelec-*
691 *tronic Engineering* **2016**, *162*, 57–62.
- 692 (48) Jürgensen, N.; Fritz, B.; Mertens, A.; Tisserant, J.-N.; Kolle, M.; Gomard, G.;
693 Hernandez-Sosa, G. A Single-Step Hot Embossing Process for Integration of Microlens
694 Arrays in Biodegradable Substrates for Improved Light Extraction of Light-Emitting
695 Devices. *Advanced Materials Technologies* **2021**, *6*, 1900933.

- 696 (49) Kunnavakkam, M. V.; Houlihan, F.; Schlax, M.; Liddle, J.; Kolodner, P.; Nalamasu, O.;
697 Rogers, J. Low-cost, low-loss microlens arrays fabricated by soft-lithography replication
698 process. *Applied physics letters* **2003**, *82*, 1152–1154.
- 699 (50) Li, M.; Yang, Q.; Bian, H.; Yang, T.; Hou, X.; Chen, F. Microlens arrays enable
700 variable-focus imaging. *Optics & Laser Technology* **2022**, *153*, 108260.
- 701 (51) Liu, J.; Chang, M.-J.; Ai, Y.; Zhang, H.-L.; Chen, Y. Fabrication of microlens arrays by
702 localized hydrolysis in water droplet microreactors. *ACS Applied Materials & Interfaces*
703 **2013**, *5*, 2214–2219.
- 704 (52) Mei, L.; Qu, C.; Xu, Z.; Wang, G.; Zhang, J.; Guo, X.; Peng, Y. Facile fabrication
705 of microlens array on encapsulation layer for enhancing angular color uniformity of
706 color-mixed light-emitting diodes. *Optics & Laser Technology* **2021**, *142*, 107227.
- 707 (53) Zhang, X.; Lu, Z.; Tan, H.; Bao, L.; He, Y.; Sun, C.; Lohse, D. Formation of surface
708 nanodroplets under controlled flow conditions. *Proceedings of the National Academy of*
709 *Sciences* **2015**, *112*, 9253–9257.
- 710 (54) Zhang, X.; Ren, J.; Yang, H.; He, Y.; Tan, J.; Qiao, G. G. From transient nanodroplets
711 to permanent nanolenses. *Soft Matter* **2012**, *8*, 4314–4317.
- 712 (55) Bao, L.; Rezk, A. R.; Yeo, L. Y.; Zhang, X. Highly ordered arrays of femtoliter surface
713 droplets. *Small* **2015**, *11*, 4850–4855.
- 714 (56) Dongare, P. D.; Alabastri, A.; Neumann, O.; Nordlander, P.; Halas, N. J. Solar thermal
715 desalination as a nonlinear optical process. *Proceedings of the National Academy of*
716 *Sciences* **2019**, *116*, 13182–13187.
- 717 (57) Lu, Q.; Xu, Q.; Meng, J.; How, Z. T.; Chelme-Ayala, P.; Wang, X.; Gamal El-Din, M.;
718 Zhang, X. Surface microlenses for much more efficient photodegradation in water treat-
719 ment. *ACS ES&T Water* **2022**, *2*, 644–657.

- 720 (58) Luo, X.; Zhan, Y.; Huang, Y.; Yang, L.; Tu, X.; Luo, S. Removal of water-soluble acid
721 dyes from water environment using a novel magnetic molecularly imprinted polymer.
722 *Journal of hazardous materials* **2011**, *187*, 274–282.
- 723 (59) Ren, S.; Li, Q.; Wang, J.; Fan, B.; Bai, J.; Peng, Y.; Li, S.; Han, D.; Wu, J.;
724 Wang, J., et al. Development of a fast and ultrasensitive black phosphorus-based
725 colorimetric/photothermal dual-readout immunochromatography for determination of
726 norfloxacin in tap water and river water. *Journal of Hazardous Materials* **2021**, *402*,
727 123781.
- 728 (60) Bahnmüller, S.; von Gunten, U.; Canonica, S. Sunlight-induced transformation of sulfa-
729 diazine and sulfamethoxazole in surface waters and wastewater effluents. *Water research*
730 **2014**, *57*, 183–192.
- 731 (61) Zhang, X. H.; Ducker, W. Formation of interfacial nanodroplets through changes in
732 solvent quality. *Langmuir* **2007**, *23*, 12478–12480.
- 733 (62) Tian, G.; Fu, H.; Jing, L.; Tian, C. Synthesis and photocatalytic activity of stable
734 nanocrystalline TiO₂ with high crystallinity and large surface area. *Journal of Haz-
735 ardous Materials* **2009**, *161*, 1122–1130.
- 736 (63) Chen, W.; Liu, Q.; Tian, S.; Zhao, X. Exposed facet dependent stability of ZnO mi-
737 cro/nano crystals as a photocatalyst. *Applied Surface Science* **2019**, *470*, 807–816.
- 738 (64) Qian, J.; Arends, G. F.; Zhang, X. Surface nanodroplets: formation, dissolution, and
739 applications. *Langmuir* **2019**, *35*, 12583–12596.
- 740 (65) Lei, L.; Li, J.; Yu, H.; Bao, L.; Peng, S.; Zhang, X. Formation, growth and applications
741 of femtoliter droplets on a microlens. *Physical Chemistry Chemical Physics* **2018**, *20*,
742 4226–4237.

- 743 (66) Makuła, P.; Pacia, M.; Macyk, W. How to correctly determine the band gap energy of
744 modified semiconductor photocatalysts based on UV–Vis spectra. 2018.
- 745 (67) Zhang, A.; Fang, Y. Influence of adsorption orientation of methyl orange on silver
746 colloids by Raman and fluorescence spectroscopy: pH effect. *Chemical physics* **2006**,
747 *331*, 55–60.
- 748 (68) Saikia, L.; Bhuyan, D.; Saikia, M.; Malakar, B.; Dutta, D. K.; Sengupta, P. Photocat-
749 alytic performance of ZnO nanomaterials for self sensitized degradation of malachite
750 green dye under solar light. *Applied Catalysis A: General* **2015**, *490*, 42–49.
- 751 (69) Ahluwalia, S.; Prakash, N. T.; Prakash, R.; Pal, B. Improved degradation of methyl
752 orange dye using bio-co-catalyst Se nanoparticles impregnated ZnS photocatalyst under
753 UV irradiation. *Chemical Engineering Journal* **2016**, *306*, 1041–1048.
- 754 (70) Lipovsky, A.; Tzitrinovich, Z.; Friedmann, H.; Applerot, G.; Gedanken, A.; Lubart, R.
755 EPR study of visible light-induced ROS generation by nanoparticles of ZnO. *The Jour-*
756 *nal of Physical Chemistry C* **2009**, *113*, 15997–16001.
- 757 (71) Li, X.; Zhang, P.; Jin, L.; Shao, T.; Li, Z.; Cao, J. Efficient photocatalytic decomposition
758 of perfluorooctanoic acid by indium oxide and its mechanism. *Environmental science*
759 *& technology* **2012**, *46*, 5528–5534.
- 760 (72) Turchi, C. S.; Ollis, D. F. Photocatalytic degradation of organic water contaminants:
761 mechanisms involving hydroxyl radical attack. *Journal of catalysis* **1990**, *122*, 178–192.
- 762 (73) Zepp, R. G.; Cline, D. M. Rates of direct photolysis in aquatic environment. *Environ-*
763 *mental Science & Technology* **1977**, *11*, 359–366.
- 764 (74) Persico, M.; Granucci, G. *Photochemistry: A modern theoretical perspective*; Springer,
765 2018.

- 766 (75) Ahmed, S.; Rasul, M.; Brown, R.; Hashib, M. Influence of parameters on the heteroge-
767 neous photocatalytic degradation of pesticides and phenolic contaminants in wastewa-
768 ter: a short review. *Journal of environmental management* **2011**, *92*, 311–330.
- 769 (76) Rafiq, A.; Ikram, M.; Ali, S.; Niaz, F.; Khan, M.; Khan, Q.; Maqbool, M. Photocat-
770 alytic degradation of dyes using semiconductor photocatalysts to clean industrial water
771 pollution. *Journal of Industrial and Engineering Chemistry* **2021**, *97*, 111–128.
- 772 (77) Wang, Z.; Ma, W.; Chen, C.; Ji, H.; Zhao, J. Probing paramagnetic species in titania-
773 based heterogeneous photocatalysis by electron spin resonance (ESR) spectroscopy—a
774 mini review. *Chemical Engineering Journal* **2011**, *170*, 353–362.
- 775 (78) Kim, Y.; Hwang, H. M.; Wang, L.; Kim, I.; Yoon, Y.; Lee, H. Solar-light photocatalytic
776 disinfection using crystalline/amorphous low energy bandgap reduced TiO₂. *Scientific*
777 *reports* **2016**, *6*, 1–10.
- 778 (79) Vinodgopal, K.; Wynkoop, D. E.; Kamat, P. V. Environmental photochemistry on
779 semiconductor surfaces: photosensitized degradation of a textile azo dye, acid orange
780 7, on TiO₂ particles using visible light. *Environmental Science & Technology* **1996**, *30*,
781 1660–1666.
- 782 (80) Yan, X.; Ohno, T.; Nishijima, K.; Abe, R.; Ohtani, B. Is methylene blue an appropri-
783 ate substrate for a photocatalytic activity test? A study with visible-light responsive
784 titania. *Chemical Physics Letters* **2006**, *429*, 606–610.
- 785 (81) Martín-Sómer, M.; Pablos, C.; van Grieken, R.; Marugán, J. Influence of light distri-
786 bution on the performance of photocatalytic reactors: LED vs mercury lamps. *Applied*
787 *Catalysis B: Environmental* **2017**, *215*, 1–7.
- 788 (82) Selvaraj, S.; Palanivel, B.; Patrick, S.; Krishna Mohan, M.; Navaneethan, M.; Pon-
789 nusamy, S.; Muthamizchelvan, C. Effect of Sr doping in ZnO microspheres for solar

- 790 light-driven photodegradation of organic pollutants. *Journal of Materials Science: Ma-*
791 *terials in Electronics* **2022**, *33*, 8777–8788.
- 792 (83) Xekoukoulotakis, N. P.; Drosou, C.; Brebou, C.; Chatzisyneon, E.; Hapeshi, E.; Fatta-
793 Kassinos, D.; Mantzavinos, D. Kinetics of UV-A/TiO₂ photocatalytic degradation and
794 mineralization of the antibiotic sulfamethoxazole in aqueous matrices. *Catalysis Today*
795 **2011**, *161*, 163–168.